

Enhanced colorimetric detection of norovirus using in-situ growth of Ag shell on Au NPs

メタデータ	言語: eng 出版者: 公開日: 2019-01-16 キーワード (Ja): キーワード (En): 作成者: Khoris, Indra Memdi, Takemura, Kenshin, Lee, Jaewook, Hara, Toshimi, Abe, Fuyuki, Suzuki, Tetsuro, Park, Enoch Y. メールアドレス: 所属:
URL	http://hdl.handle.net/10297/00026251

Enhanced colorimetric detection of norovirus using in-situ growth of Ag shell on Au NPs

Indra Memdi Khoris^a, Kenshin Takemura^b, Jaewook Lee^{c, †}, Toshimi Hara^d, Fuyuki Abe^d, Tetsuro Suzuki^e, Enoch Y. Park^{*, a, b, c}

^a *Department of Applied Biological Chemistry, College of Agriculture, Graduate School of Integrated Science and Technology, Shizuoka University, 836 Ohya, Suruga-ku, Shizuoka 422-8529, Japan*

^b *Department of Bioscience, Graduate School of Science and Technology, Shizuoka University, 836 Ohya, Suruga-ku, Shizuoka 422-8529, Japan*

^c *Research Institute of Green Science and Technology, Shizuoka University, 836 Ohya, Suruga-ku, Shizuoka 422-8529, Japan*

^d *Department of Microbiology, Shizuoka Institute of Environment and Hygiene, 4-27-2, Kita-ando, Aoi-ku, Shizuoka 420-8637, Japan*

^e *Department of Infectious Disease, Hamamatsu University School of Medicine, 1-20-1 Higashi-ku, Handa-yama, Hamamatsu 431-3192, Japan*

E-mail:

indra.memdi.khoris.17@shizuoka.ac.jp (IMK)

takemura.kenshin.16@shizuoka.ac.jp (KT)

nanojaewook@outlook.com (JL)

toshimi1_hara@pref.shizuoka.lg.jp (TH)

fuyuki1_abe@pref.shizuoka.lg.jp (FA)

tesuzuki@hama-med.ac.jp (TS)

park.enoch@shizuoka.ac.jp (EYP)

* Corresponding author: Research Institute of Green Science and Technology, Shizuoka University, 836 Ohya, Suruga-ku, Shizuoka 422-8529, Japan.

E-mail address: park.enoch@shizuoka.ac.jp (E.Y. Park). Tel (Fax): +81-54-238-4887

† Current address; School of Materials Science, Japan advanced Institute of science and Technology, Asahidai 1-1, Nomishi, Ishikawa 923-1292, Japan

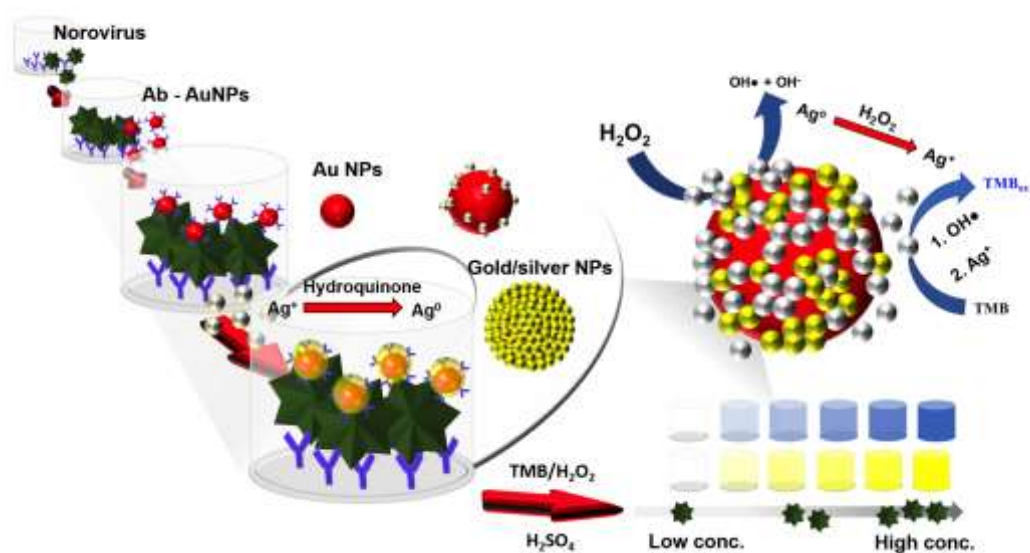
Abstract

Norovirus (NoV) is a leading cause of acute gastroenteritis. The low infectious dose and environmental stability of NoV facilitate its effective transmission through a variety of modes such as food, water and person-to-person. The available enzyme-linked immunosorbent assay (ELISA) for NoV detection has low sensitivity due to the low catalytic activity of the peroxidase used, and thus, a reliable ultrasensitive bioassay is needed. In this study, we apply the enhanced peroxidase-like activity of silver ion-incorporated gold nanoparticles (Au/Ag NPs) in a colorimetric bioassay for NoV detection. NoV was captured by anti-NoV genogroup II antibodies, which were immobilized on the surface of a 96-well microtiter plate and formed a sandwich structure among anti-NoV Ab, NoV and Ab-Au NP. Then, Ag ion-containing hydroquinone was added to form Au/Ag core/shell NPs. When H₂O₂/3,3',5,5'-tetramethylbenzidine (TMB) solution was added to the wells, Ag ions were liberated from the surface of Au/Ag NPs and enhanced the oxidation of TMB. These reactions enhanced the oxidation of TMB and developed an intense blue color. The Au/Ag NPs were shown to exhibit higher affinity and catalytic efficiency for H₂O₂ and higher catalytic velocity based on the *k_{cat}* of up to 7-fold compared with Au NPs. The bioassay was then optimized to detect clinically isolated NoV using NoV-like particles (NoV-LPs). NoV-LPs were detected with a limit of detection of 10.8 pg/mL, corresponding to 1000- and 100-fold higher sensitivity compared to the gold-immunoassay and horseradish peroxidase-based ELISA, respectively. Clinically isolated NoV GII.4 and NoV GII.3 were detected in the range of 10²–10⁶ copies of viral RNA/mL fecal solution with a detection limit of 13.2 copies/mL fecal solution for NoV GII.4, equivalent to 132 copies of viral RNA/g feces and indicating significantly higher sensitivity compared to commercial immunoassay kits. This bioassay

represents a workable detection assay for low concentrations of NoV that is applicable for early-stage diagnosis for public hygiene.

Keywords: Colorimetric bioassay, Norovirus, Norovirus-like particles, Peroxidase-like activity, Gold/silver nanohybrid.

Graphical abstract



1. Introduction

Public awareness of health and well-being is increasing dramatically due to the increase in life expectancy (Caliendo et al. 2013; Mays and Smith 2011; Neethirajan et al. 2017). To satisfy public needs and the desire for health, rapid and highly sensitive biosensing systems are required to detect infectious viruses and prevent the spread of virus-derived infectious diseases (Caygill et al. 2010; Hao et al. 2017; Zhou et al. 2017). Populated countries, such as China and India, as well as developing countries with remote settings and limited resources have driven biosensor research to produce simple, easy-to-perform and low-cost sensing platforms (Vashist et al. 2015).

In several countries, including Japan, England, the US, China, Australia and Russia, norovirus (NoV) infection occurs in the food industry during the winter season (de Graaf et al. 2015), and NoV is considered a serious risk to public hygiene. This disease is the main pathogenic virus responsible for nonbacterial acute gastroenteritis (Patel et al. 2009). Based on the Infectious Agents Surveillance Report for February 2017, cases of gastroenteritis by NoV re-emerged in Japan in 2015 and 2016. NoV infection occurs in the epithelium of the human small intestine. Although usually moderate, clinical symptoms including diarrhea and vomiting; occasionally, fever, headaches and abdominal pain can be severe and last longer in young children and the elderly (Hall et al. 2011). NoV can infect at a low infectious dose of approximately 100 virus particles/mL (Yakes et al. 2013) and is spread easily through food and water, as well as by the vomit and stool of infected persons (Hwang et al. 2017).

Several well-known NoV detection methods are based on polymerase chain reaction (PCR) and ELISA. PCR-based RNA detection has been used to identify NoV and is

considered the gold standard. However, this method requires expensive equipment and a well-trained technician to operate it. ELISA kits are available but are not appropriate for early-stage diagnosis due to low sensitivity. Horseradish peroxidase (HRP) has been used in ELISA kits to catalyze the reduction of a chromogenic (colorimetric) agent by hydrogen peroxide (Aydin 2015). HRP shows a loss of activity at high peroxide concentration such as those found in phenol, hydrogen peroxide and nitrites, and also in harsh physicochemical environment (Baynton et al. 1994; Samuni et al. 2017). This leads to a limit on the degree of signal amplification for application and requires the development of alternative enzyme-like materials.

Recently, several nanomaterials have been developed as potential candidates with enzyme-like activity, such as ferromagnetic nanoparticles that exhibit peroxidase-mimic activity (Gao et al. 2007). In other studies, various nanomaterials have been investigated, such as metals and their derivatives, including metal oxides or sulfides (Dai et al. 2009), metal coenzyme nanostructures (Lee et al. 2018), and carbon-based nanostructures (Ahmed et al. 2016b; Zheng et al. 2013), as well as hybrid nanomaterials such as graphene-gold hybrids (Ahmed et al. 2017) that have intrinsic catalytic activity. Gold nanoparticles (Au NPs) shows high catalytic activity and have good compatibility with most biomolecules covalently or noncovalently. However, biomolecule-modified Au NPs exhibit low catalytic activity and sensitivity due to the hindrance of the biomolecules on the surface of the Au NPs (Wang et al. 2016).

To overcome this bottleneck and achieve a highly sensitive nanozyme-based immunoassay for NoV detection, in this study, a new detection strategy was investigated with gold and silver nanohybrid nanoparticles. Silver has been used in various

applications with Au NPs, such as surface-enhanced Raman scattering detection (Xu et al. 2004), mass spectrometry (Liu et al. 2011) and opacity densitometry (Gupta et al. 2007). In our study, to obtain highly enhanced peroxidase-like activity for excellent detection performance, a silver-coated Au NP core/shell nanohybrid structure was prepared via in-situ growth in virus-sensing chamber. In addition, a capture-sandwich immunoassay for virus detection was demonstrated with hydrogen peroxide and 3,3',5,5'-tetramethylbenzidine (TMB) as the substrate and chromogenic agent, respectively. Based on our results, the sensing mechanism and the amplified color intensity via enhanced catalytic activity of Au/Ag NPs were investigated. Furthermore, the selectivity of this sensing system was confirmed, and the enhanced colorimetric immunoassay for NoV detection was demonstrated using a low-cost technique with a promising mechanism for catalytic activity using in-situ growth of Au/Ag NPs.

2. Materials and methods

2.1. Materials

Gold (III) chloride trihydrate ($\text{HAuCl}_4 \cdot 3\text{H}_2\text{O}$), bovine serum albumin (BSA), silver nitrate (AgNO_3) and cysteamine were obtained from Sigma-Aldrich (St. Louis, MO, USA). Influenza virus A/Hongkong/H9N2 was obtained from ProSpec-Tany Technogene, Ltd. (East Brunswick, NJ, USA). 3,3',5,5'-Tetramethylbenzidine (TMB) was obtained from Dojindo (Osaka, Japan). Dimethyl sulfoxide (DMSO), tween-20, hydrogen peroxide (H_2O_2), skimmed milk powder, hydroquinone (HQ), sodium acetate and sodium borohydride (NaBH_4) were purchased from Wako Pure Chem., Inc. (Osaka, Japan). A $10 \times$ phosphate-buffered saline (PBS) solution was prepared in 1 L by mixing 80 g of

sodium chloride, 2 g of potassium chloride, 11.5 g of sodium hydrogen phosphate, and 2 g of potassium dihydrogen phosphate in which all the reagents were purchased from Wako Pure Chem., Inc. (Osaka, Japan). All experiments were conducted using deionized (DI) water.

2.2. Biological materials and fecal sample preparation

An anti-NoV antibody broadly reactive to genogroup II (NS14 Ab) was used in this work (Kitamoto et al. 2002; Kou et al. 2015). Norovirus-like particles (NoV-LPs) were prepared according to the standard method of virus-like particle preparation (Ahmed et al. 2017). Clinically isolated NoVs were collected from fecal samples of patients with infectious gastroenteritis, including foodborne illness, as determined by inspections based on laws and ordinances. A 0.1-g quantity of fecal sample was suspended in 900 μ L of PBS (pH 7.4); after separation of the solids, the supernatant was used as the detection sample. NoV sampling was performed according to guidelines after obtaining approval from the Ethics Committee of the Environment and Hygiene Institute in Shizuoka Prefecture (September 14, 2016). The clinically isolated NoVs were assayed using a commercial NoV detection kit (NV-AD III, Denka Seiken Co., Ltd. Tokyo, Japan) for comparison.

2.3. Preparation of Au NPs and NS14 antibody-conjugation

Au NPs were synthesized by the citrate reduction method (Liu et al. 2011). Briefly, 40 mL of 0.5 mM $\text{HAuCl}_4 \cdot 3\text{H}_2\text{O}$ was boiled and stirred for 30 min, and then 1 mL of 2% (w/v) trisodium citrate trihydrate was added to the Au ion solution. The color of the solution changed from pale yellow to colorless and gradually to red-wine color. After the

color change, the solution was stirred for an additional 10 min. The solution was then cooled to room temperature and stored at 4°C. The concentration was determined based on localized surface plasmon resonance from the UV-Vis absorbance spectrum (Haiss et al. 2007). Silver nanoparticles (Ag NPs) were synthesized using a similar method with silver nitrate (25 mM) as the precursor. Five mM of trisodium citrate trihydrate and 0.025 mM of tannic acid were used as the reducing agents (Bastús et al. 2014).

To conjugate the surface of Au NPs with NS14 Ab, 10 µL of NS14 Ab (0.3 µg/mL) was added to 1 mL of Au NPs (0.76 nM) in DI water. The solution was stirred gently for 1 h, and 400 µL of 10% BSA solution was added to block the remaining surface of the Au NPs to ensure minimum nonspecific binding. The solution was stirred for 1 h. Then, the solution was centrifuged at 10,000 g for 10 min at 4°C. The suspension of NS14 Ab-conjugated Au NPs (NS14 Ab-Au NPs) was redispersed in 0.5 × PBS solution (containing 0.5% BSA, pH7.4) and stored at 4°C.

2.4. In-situ synthesis of Au/Ag NPs

Au/Ag nanohybrid NPs were synthesized by the in-situ growth method of silver deposition on the surface of Au NPs (0.76 nM) in DI water. Briefly, 1 mL of AuNPs was mixed with 1 mL of AgNO₃ (1 mM) and HQ (1 mM) (1:1 v/v) and incubated for 10 min at room temperature. After reaction, a color change from wine red to reddish orange was clearly observed. The resulting mixture was then purified by centrifugation at 9,000 g for 10 min at 4°C.

2.5. Physicochemical analysis of Au/Ag NPs

The physicochemical properties of Au/Ag NPs and Au NPs were investigated. The absorbance was measured using a clear transparent cuvette ($l = 10$ mm) in a UV-vis spectrophotometer (UV-1800, Shimadzu, Kyoto, Japan). The zeta potential and hydrodynamic size distribution (DLS) were measured in DI water using a clear, disposable zeta cell (DTS1061) using a Malvern Zetasizer (Nano-ZS, Malvern, UK). Fourier transform infrared (FT-IR) spectroscopy analysis was conducted with an FT-IR 6300 (JASCO, Tokyo, Japan). Morphology of nanoparticles was generated using a transmission electron microscope (TEM) (JEM-2100F, JEOL, Ltd., Tokyo, Japan) operated at 100 kV for AuNP, and HR-TEM images were generated using a JEM-2100F (JEOL, Ltd., Tokyo, Japan) operated at 200 kV for Au/Ag NPs. XRD analysis was performed using powder X-ray diffraction (PXRD) (RINT ULTIMA, Rigaku, Corp., Tokyo, Japan).

2.6. Catalytic activity assay

Steady-state kinetic measurements were performed by monitoring the change in absorbance of the charge transfer complex of TMB at 655 nm. In addition, the catalytic activity of Au/Ag NPs was determined from the time-dependent absorbance at 655 nm with various initial concentrations of H₂O₂ and TMB. The measured absorbance versus time plots were obtained at a fixed concentration of one substrate versus varying concentrations of the other substrate. The concentration ranges of H₂O₂ and TMB were 0.1–5.0 M in DI water and 0.1–5.0 mM in DMSO, respectively. The Michaelis–Menten constant (K_m) was calculated using Lineweaver–Burk plots of the double reciprocal of the

Michaelis–Menten equation (equation 1), where v is the initial velocity, v_m is the maximal reaction velocity, $[S]$ is the concentration of substrate. k_{cat} was calculated by equation 2.

$$\frac{1}{v} = \frac{k_m}{v_m} \left(\frac{1}{[S]} + \frac{1}{k_m} \right) \quad (\text{equation 1})$$

$$k_{cat} = \frac{v_m}{[nanozyme]} \quad (\text{equation 2})$$

The catalytic activity of the Au NPs and Au/Ag NPs was studied using dilution series of concentration. The initial concentration of the nanomaterials was 0.76 nM to 6 pM in a twofold dilution series. $[H_2O_2]$ and $[TMB]$ were 5.7 M and 2.67 mM, respectively. The reaction time was less than 1 min, and the reaction was stopped with the addition of 10% H_2SO_4 . The absorbance was measured using a microplate reader at 450 nm with a reference wavelength of 655 nm.

2.7. Enhanced colorimetric detection of NoV

The Au/Ag nanohybrid-based virus-sensing system was demonstrated via interaction between captured Ab and NoV-LPs as a model of NoV. First, 100 μ L of NS14 Ab (100 ng/mL) in PBS was immobilized in the wells of the microtiter plate overnight. The wells were washed three times with 250 μ L of $1 \times$ PBS with 0.1% Tween-20 (PBS-T) three times after each step. After immobilization of Ab, the remaining parts of the wells were blocked with 5% skimmed milk in PBS for 2 h. Subsequently, various concentrations of NoV-LPs in PBS were introduced for 1 h, and then 100 μ L of NS14 Ab-Au NPs was added and incubated for 1 h. During this stage, the captured NoV-LPs were bound to the NS14 Ab-Au NPs, and the sandwich structure was formed.

Then, 100 μL of a mixture of AgNO_3 (1 mM) and HQ (1 mM) (1:1 v/v) in DI water was added to the solution containing the NS14 Ab/NoV-LP/NS14 Ab-Au NPs sandwich structure to develop the Ag shell on the Au NPs. The Ag ions were reduced on the surface of the Au NPs via the reduction potential of HQ and the galvanic potential between the Ag ions and Au. As a result, the Ag shell was coated on the surface of Au NPs by in-situ growth within 15 min. After intense washing using $1 \times$ PBS-T followed by DI water, 100 μL containing 9 M H_2O_2 and 40 mM TMB solution (9:1 v/v) was added to the solution containing the Au/Ag-NS14 Ab-(NoV-LP)-NS14 Ab sandwich structure. Blue color quickly developed. After a reaction time of 1 min, 10% H_2SO_4 solution was added to the wells to stop the reaction, and the blue color turned to yellow. Finally, the color intensity was measured using a microplate reader (Model 680, Bio-Rad, Hercules, CA) at 450 nm. This Au/Ag nanohybrid-based virus-sensing system was optimized using NoV-LPs and applied to detect NoV according to the optimized protocol.

3. Results and discussion

3.1. Detection mechanism of the sensing platform

This Au/Ag-based colorimetric sensing platform was established under two concepts: the first was to capture the target virus using gold probes; the second was to enhance the catalytic activity using silver ions. The mechanism of virus detection is illustrated in **Scheme 1**. First, the NS14 Ab was immobilized in the wells of the plate via physical adsorption. Then, the target virus was introduced in the sensing chamber (I). Subsequently, NS14 Ab-Au NPs were added to the mixture to form the sandwich structure (II). Next, Ag ions and HQ were added to produce the in-situ Ag-coated Au NP

structure to obtain enhanced catalytic activity (III). The Au NPs functioned as a seed, and the Ag shell was automatically grown on the surface of the Au NPs by the in-situ growth method. After removing excess silver solution by washing thoroughly with DI water, H₂O₂/TMB solution was introduced to the wells, and an intense blue color was developed due to the synergic effect of the peroxidase-like activity of Au/Ag nanohybrid (IV). After 1 min, 10% H₂SO₄ was added to stop the reaction, and a proportional yellow color was developed (V). Finally, the absorbance at 450 nm was measured to determine the sensitivity and selectivity of this detection system.

3.2. Characteristics of Au NPs and Au/Ag nanohybrid NPs

The morphology and size of the Au/Ag nanohybrid NPs were observed by using TEM. Before the core/shell reaction, the size of the Au NPs seed was approximately 12 nm (**Fig. 1A**). However, after silver deposition by adding Ag⁺/HQ solution, double-layered particles with a size of 27 nm were clearly observed by high-resolution TEM imaging (**Fig. 1B**). The boundary was noticeable (**Fig. 1B**) due to the difference in electron density between the darker part corresponding to Au NPs (14 nm) (red arrow) and the lighter part corresponding to the deposited silver around the Au NPs (yellow arrow). The particles showed an Au/Ag core/shell structure with homogeneous growth judging from the images in **Fig. 1B**. In addition to TEM images, as shown in **Fig. S1**, EDS spectra of the Au/Ag nanohybrid corresponding to Au (M) and Ag (L) supported the presence of the elements in the nanohybrid.

The optical properties of the Au/Ag nanohybrid NPs were characterized by using UV/Vis spectroscopy. The Au NP seeds showed one plasmonic absorbance (black curve) near 525 nm. However, after the core/shell reaction, a new plasmonic band (red curve)

appeared at approximately 398 nm (**Fig. 1C**), indicating that the Ag shell was successfully deposited on the surface of the Au NPs. Interestingly, the Au plasmonic band was blueshifted to approximately 490 nm in the Au/Ag nanohybrid formation (Banerjee et al. 2011). Moreover, the zeta potential and hydrodynamic size were measured to silver shell formation. The influence of the concentration of Ag ions in the silver shell precursor was assessed at a constant concentration of Au NPs by monitoring the changes in the zeta potential and hydrodynamic size in a 15-min reaction. Initially, the Au NPs had a surface charge, with a zeta potential of approximately -38 mV, and a hydrodynamic size of 18 nm (**Fig. 1D**). As the concentration of Ag ions increased, the zeta potential of the Au NPs became less negative and relatively constant at -10 mV; simultaneously, the hydrodynamic size increased from 18 nm to 30 nm. Moreover, the addition of silver nitrate reached saturation of silver shell formation as indicated by the near-constant increase in size measured by DLS analysis. lattice parameter and structural analyses of Au and Au/Ag were conducted by using XRD (**Fig. 1E**). The diffraction pattern of (111) was obtained at approximately 37 degrees for both Au NPs and the Au/Ag nanohybrid. However, the pattern of (200) was measured at different angle: 44 degrees for Au NPs and 46 degrees for the Au/Ag nanohybrid. In addition, the other diffraction patterns of the Au NPs disappeared after the core/shell reaction, indicating that the Au was completely covered by the Ag layer. Consequently, the pattern of the Ag-oriented crystal structure was measured in the Au/Ag nanohybrid structure by XRD.

3.3. Kinetic parameters of the catalytic activity of Au/Ag NPs and Au NPs

The steady-state kinetic approximation was introduced to investigate the enhanced peroxidase-like activity of Au/Ag NPs, and the kinetic parameters and catalytic efficiency

were evaluated in terms of k_{cat}/K_m . The kinetic parameters v_m and K_m were determined by using various concentrations of the substrates, H_2O_2 and TMB. To calculate the initial velocity of the nanomaterials for each substrate, H_2O_2 and TMB, the time-based absorbances of both nanomaterials were collected. The initial velocity was plotted on the y-axis, and the concentration of substrate was plotted on the x-axis (Michelin-Menten relationship). The kinetic parameters were determined by analyzing the double-reciprocal form (Lineweaver-Burk plot) (**Fig. S2**) with $1/[S]$ as the x-axis and $1/[v]$ as the y-axis. k_{cat} was determined by dividing the calculated v_m by [nanozyme]. The concentration of Au/Ag NPs was based on the initial concentration of Au NPs. These assumptions were used to show the role of the silver shell in enhancing the activity of the Au core, and the actual concentration of the Au/Ag NPs will not exceed the initial concentration of Au NPs in terms of Au itself. As shown in **Table 1**, the K_m values of Au/Ag NPs for TMB and H_2O_2 were significantly lower than those of Au NPs, with differences of 10 times and 40 times, respectively. These results show the high affinity of the Au/Ag NPs toward both substrates. Moreover, the comparison of enzyme efficiency (k_{cat}/K_m) revealed interesting comparison of both nanomaterials toward the substrate. Both Au/Ag NPs and Au NPs had similar efficiency values for TMB due to their negative charge, which confers high binding affinity with the diamine group of TMB (Wang et al. 2012). By contrast, for H_2O_2 , Au/Ag NPs showed 2 times higher catalytic efficiency compared to Au NPs. Further comparing the enzymatic efficiency between the substrates showed that the Au NPs had a lower activity preference for H_2O_2 than for TMB. By contrast, the Au/Ag NPs exhibited an activity preference to H_2O_2 compared with TMB due to the phenomenon of enhancement by the silver shell on the surface of the Au NPs. Based on the kinetic

parameters of the nanomaterials toward the substrates H₂O₂ and TMB, Au/Ag NPs exhibit more efficient catalytic activity and higher substrate affinity than Au NPs.

Furthermore, the maximal reaction velocity (v_m) was compared between Au/Ag NPs and Au NPs. The Au/Ag NPs and Au NPs were diluted in series and introduced to H₂O₂/TMB in microplate wells (250 μ L), and the absorbance was measured after a defined reaction time ($t = 1$ min) to compare the catalytic activity and enzymatic behavior. Because the substrate concentrations were sufficiently high compared to K_m , at a low concentration of nanozyme, the reaction velocity (v) can be assumed to equal v_m . (Berg et al. 2002). The catalytic activity assay of the nanomaterials was plotted as [nanozyme] vs maximal reaction rate of oxidized TMB (**Fig. 2A**). Based on the Beer-Lambert law, the slope of the linear line can be defined as k_{cat} within the linear range of the plot. The values of k_{cat} for Au NPs and Au/Ag NPs were $5.58 \times 10^4 \text{ s}^{-1}$ and $4.67 \times 10^5 \text{ s}^{-1}$, respectively (the molar coefficient of TMB_{ox} is $6 \times 10^4 \text{ M}^{-1} \cdot \text{cm}^{-1}$). The comparison of the k_{cat} values indicates that the turnover of Au/Ag NPs is 7-fold higher than that of Au NPs.

3.4. Interfering effect of protein on the surface of NPs on catalytic activity

Although the incorporation of silver on the Au NPs was shown to increase catalytic activity and affinity for H₂O₂, a drawback is that the active sites of Au NPs can be blocked with protein, because of covering active site of NPs by BSA which is commonly used to reduce the nonspecific binding of NPs (Byzova et al. 2017). Centrifuged Au NPs and Au/Ag NPs were incubated with various concentration of BSA to form protein-blocked Au NPs (Au/protein NPs) and Au/Ag NPs (Au/Ag/protein NPs), respectively. The effect of blocking on the catalytic activity of each of the NPs was assayed (**Fig. S3**). NPs were incubated at a defined BSA concentration and centrifuged to separate the uncoated BSA.

Peroxidase-like activity was then measured. Both Au/protein NPs and Au/Ag/protein NPs showed a greater than 60% interfering effect of protein on the surface of the NPs. Au/Ag NPs were prepared in situ as follow. The BSA-coated Au NPs were applied to Ag^+ /HQ (1/1 mM) solution to form the silver shell on the surface of the Au NPs. The interfering effect of protein on the catalytic activity of the in-situ Au/Ag NPs was less than 40% (**Fig. S3**). This result clearly demonstrated that the peroxidase active of Au/protein/Ag NPs were less influenced by the physically absorbed protein compared to those of Au/Ag/protein NPs and Au/protein NPs. The protein-coated Au NPs and Au/Ag NPs lose active sites on the metal surfaces due to the coverage of the physically adsorbed protein, resulting in reduced catalytic activity (**Fig. 2B**). However, in situ silver-deposition on the protein-coated Au NPs (Au/protein/Ag NPs) showed higher activity than Au/Ag NPs and Au NPs in the presence of protein. This Ag shell provides new active catalytic sites, resulting in significant enhancement of the catalytic activity even in the presence of protein (**Fig. 2B**), which was applied to enhance the colorimetric immunoassay.

3.5. Silver ion-enhanced peroxidase-like activity of Au/Ag NPs

The catalytic activity of Au/Ag NPs is a key factor for the TMB- and H_2O_2 -based colorimetric biosensing assay because the interaction between TMB and H_2O_2 , which is the basis of the color change, is catalyzed by Au/Ag NPs which function as a nanozyme. Based on the kinetic parameter results, silver deposition increases the affinity of the nanomaterials for H_2O_2 . The reactivity of the nanohybrid was further investigated in H_2O_2 solution without TMB by simply using a UV-Vis spectrophotometer. In a short time, a distinguishable change in the absorbance spectrum of the Au/Ag NPs was observed, as shown in **Fig. S4A**. Time-based measurements were performed and revealed gradually

increasing absorbance at 399 nm and a blueshift of the absorbance at 520 nm, indicating stepwise silver deposition on the surface of Au seeds. The blueshift was induced by plasmonic interaction between Au and Ag in the Au/Ag nanohybrid. **Fig. 3A** illustrates the process of formation of the Au core/Ag shell structure. The nanohybrid was then exposed to H₂O₂ solution, and the rapid decomposition of the Ag shell was monitored based on the change in the absorbance spectrum at 390 nm and the redshift of the peak from 499 nm to 520 nm (**Fig. S4B**). The color returned to red-wine from reddish orange. The rapid Ag-shell dissociation into Ag ions (**Fig. 3B**) was evident by the enhancement of the peroxidase-like activity, which requires the generation of radical species and silver ions.

The Ag reaction with peroxides involves an autocatalytic reaction of Ag/Ag⁺ and H₂O₂ (Bhagat et al. 2018; He et al. 2012a; He et al. 2012b; Hou et al. 2018; Jones et al. 2011; Ni et al. 2015; Parnklang et al. 2015). The entire reaction, including activation of H₂O₂, radical generation and TMB oxidation, is summarized in **Table S1**. The Ag ions were released from the Au/Ag hybrid structure via H₂O₂ (Reaction 1 in **Table S1**), and because of the galvanic potential difference between Au and Ag, the dissociation of Ag ions was enhanced (Alissawi et al. 2013). Hence, silver was oxidized to silver ions with hydroxyl ions and hydroxyl radical, and the hydroxyl ion further reacted with H₂O₂ in an acid-base Lewis reaction to form hydroperoxyl ion (HOO⁻). In this redox system, TMB was oxidized by 3 factors: first, the OH⁻ radical from the reaction between Ag and H₂O₂ (Reaction 1 in **Table S1**); second, the OH⁻ radical from H₂O₂ catalyzed by Au NPs; third, the reduction potential from Ag⁺ ions (Reactions 2 and 3 in **Table S1**). Thus, the color development via oxidation of TMB was accelerated by multiple effects of the Au/Ag NPs. As the potential oxidants of TMB present in the reaction increased, the colorimetric

sensing platform was enhanced. Only Ag NPs was also assayed in the H₂O₂/TMB system. As shown in **Fig. S5A**, TMB was rapidly oxidized in presence of Ag NPs and Au/Ag NPs, and slower if only AuNPs were presence. This showed the major point in this enhancement system came from the reaction of Ag shell with H₂O₂/TMB, not Au core. In addition, Ag NPs alone were assayed to show the catalytic activity over time at several concentrations. Interestingly, the charge complex of TMB (measured in A₆₅₅) were not sustained, and consequently the color that developed was not stable, compared to color developed by Au/Ag NPs (**Fig. S5B**). After all Ag NPs was decomposed to Ag⁺ and reacted to TMB, the oxidation was stopped, however, it is not the case in Au/Ag NPs. These results showed interesting catalytic activity of TMB oxidation using Au/Ag NPs than Ag NPs for colorimetric system.

3.6. In-situ growth of the Au/Ag nanohybrid in the gold nanozyme-based immunoassay

To demonstrate the enhanced colorimetric immunoassay via in-situ Au/Ag NPs, Ag ion solution containing HQ was added to the well containing the sandwich form, i.e., NS14 Ab/NoV-LP/NS14 Ab-Au NPs. Chromogenic solution including H₂O₂/TMB was added to the nanohybrid system. Immediately, a blue color developed due to the catalytic activity of the nanohybrid, and after a few minutes, the reaction was stopped by the addition of H₂SO₄ stop solution, which resulted in a change in color from blue to yellow. The concentration of silver ion (AgNO₃) and hydroquinone, was optimized to ensure minimum independent growth or nonspecific deposition of silver nanoparticles in the wells. A sufficiently high concentration of the silver ions as a precursor of the silver shell and hydroquinone as a reducing agent for the deposition of silver in the well could lead to Ag NP formation without the presence of Au seeds. As shown in **Fig. S6**, a background

signal was observed in the wells without Au NPs. The background signal increased at concentrations higher than 1 mM. Although the response of the catalytic activity from the in-situ formed Au/Ag nanohybrid increased (gray bars of **Fig. S6**), the error bars also increased, indicating instability of the assay at higher amounts of silver precursor. The higher background and error bar showed that 1 mM was a reasonable and optimized concentration of silver enhancement solution (Ag^+ and HQ). In this work, washing step is required, especially between before and after the addition of Ag^+ /HQ solution. The effect of the washing solution on the silver enhancement in the assay was assessed. Due to the high ionic strength of the washing buffer, in this case PBS-T, the Ag ion formed AgCl and finally precipitated (**Fig. S7**). In addition, high background was unavoidable. As a result, the washing before the Ag enhancement step was performed with additional DI water only. To obtain better assay results, the washing step was conducted by three times PBS-T and two additional DI water to rinse remaining free ions (Gupta et al. 2007).

3.7. Enhanced colorimetric immunoassay of NoV

Based on the results of the catalytic activity of the in-situ Au/Ag NPs, the colorimetric immunoassay of NoV-LPs as a model of NoV was carried out. First, NS14 Ab conjugation on Au NPs was confirmed using a conventional ELISA system with IgG-HRP (**Fig. S8**). The selectivity of this sensing system was assessed with several biological agents such as influenza virus and BSA. As shown in **Fig. 4A**, only the wells containing NoV-LPs showed an intense yellow color. This result demonstrated that the NS14 Ab-Au NPs did not bind to other viruses or proteins due to the specificity of the antibodies and blocking process. The sensitivity of this sensing system was evaluated by monitoring the color change as a function of the concentration of NoV-LPs. A linear response was

obtained as a function of the concentration of NoV-LPs with a correlation coefficient (R^2) of 0.965 (**Fig. 4B**). In addition, the calculated limit of detection (LOD) (Ahmed et al. 2016a) was approximately 10.8 pg/mL. However, the visibility of the color developed by Au NPs without the addition of Ag^+ /HQ solution was 1000-fold lower due to the blocking process on the Au NPs (Wang et al. 2016). Moreover, HRP-based ELISA showed a higher response than the Au NPs system, but the system was only usable for high concentrations of NoV-LPs due to its up to 100-fold poorer sensitivity compared to the proposed Au/Ag nanozyme. Interestingly, as shown in **Fig. S9**, the concentration of NoV-LPs could be assayed by distinguishing yellow color development by the naked eye, indicating that this proposed method is a promising enhanced immunoassay that is superior to HRP-based ELISA.

Furthermore, to show its practical application, the proposed assay was used to detect clinically isolated NoVs obtained from human feces. As shown in **Fig. 5**, the absorbance response increased based on the NoV concentration (in copies/mL). The inset images show the increasing color intensity with increasing NoV concentration. Compared with the commercial NoV detection kit, the response was significantly enhanced. The proposed assay was used to detect NoV GII.4 (**Fig. 5A**) and NoV GII.3 (**Fig. 5B**), and the detection results were compared with those of the commercial NoV detection kit. Both showed increasing color change as a response to increasing NoV concentration. The proposed assays showed a color change at 10^2 and 10 copies of viral RNA/mL of fecal sample for NoV GII.4 and GII.3, respectively, whereas the commercial NoV detection kit detected 10^6 copies of viral RNA/mL. The silver enhanced immunoassay showed a limit of detection of 16.3 copies of viral RNA/mL (163 copies of viral RNA/g feces) for NoV GII.4 and 13.2 copies of viral RNA/mL (132 copies of viral RNA/g feces) for NoV GII.3.

4. Conclusion

Au/Ag NPs significantly enhanced peroxidase-like activity as a nanozyme. Silver deposition on the gold surface increased the affinity of the nanohybrid for H₂O₂ and simultaneously enhanced the reaction with TMB due to the increase in more available reactive species. This immunoassay showed high sensitivity and selectivity for NoV detection. The detection limits of the developed assay for NoV-LPs and NoV were 10.8 pg/mL in the range of 1 pg/mL–100 ng/mL and 13.2 copies of viral RNA/mL (132 copies/g feces) in the range of 10²–10⁶ copies of viral RNA/mL, respectively, and a positive reaction was detectable by the naked eye. Due to the greater visible color intensity for detection, this enhancement method could be used with other antibodies in the nanozyme to create colorimetric assays for excellent monitoring systems to promote public hygiene.

Acknowledgement

JL thanks the Japan Society for the Promotion of Science (JSPS) for a postdoctoral fellowship (No. P16361). This work was supported in part by the Bilateral Joint Research Project of the JSPS, Japan.

Conflict of interest

The authors declare no competing financial interest.

Appendix A. Supporting information

Supplementary data associated with this article can be found in the online version at <http://dx.doi.org/>.

References

- Ahmed, S.R., Kim, J., Suzuki, T., Lee, J., Park, E.Y., 2016a. *Biotechnol. Bioeng.* 113(10), 2298–2303.
- Ahmed, S.R., Kim, J., Suzuki, T., Lee, J., Park, E.Y., 2016b. *Biosens. Bioelectron.* 85, 503–508.
- Ahmed, S.R., Takemeura, K., Li, T.-C., Kitamoto, N., Tanaka, T., Suzuki, T., Park, E.Y., 2017. *Biosens. Bioelectron.* 87, 558–565.
- Alissawi, N., Zaporojtchenko, V., Strunskus, T., Kocabas, I., Chakravadhanula, V., Kienle, L., Garbe-Schönberg, D., Faupel, F., 2013. *Gold Bull.* 46(1), 3–11.
- Aydin, S., 2015. *Pept.* 72, 4–15.
- Banerjee, M., Sharma, S., Chattopadhyay, A., Ghosh, S.S., 2011. *Nanoscale* 3(12), 5120–5125.
- Bastús, N.G., Merkoçi, F., Piella, J., Puntès, V., 2014. *Chem. Materials* 26(9), 2836–2846.
- Baynton, K.J., Bewtra, J.K., Biswas, N., Taylor, K.E., 1994. *Biochim. et Biophys. Acta (BBA)-Protein Struct. and Mol. Enzym.* 1206(2), 272–278.
- Berg, J., Tymoczko, J., Stryer, L., 2002. *Biochem.* 5.
- Bhagat, S., Vallabani, N.S., Shutthanandan, V., Bowden, M., Karakoti, A.S., Singh, S., 2018. *J. Colloid Interface Sci.* 513, 831–842.
- Byzova, N.A., Safenkova, I.V., Slutskaya, E.S., Zherdev, A.V., Dzantiev, B.B., 2017. *Bioconjug. Chem.* 28(11), 2737–2746.
- Caliendo, A.M., Gilbert, D.N., Ginocchio, C.C., Hanson, K.E., May, L., Quinn, T.C., Tenover, F.C., Alland, D., Blaschke, A.J., Bonomo, R.A., Carroll, K.C., Ferraro,

- M.J., Hirschhorn, L.R., Joseph, W.P., Karchmer, T., MacIntyre, A.T., Reller, L.B., Jackson, A.F., 2013. *Clin Infect Dis* 57 Suppl 3, S139–170.
- Caygill, R.L., Blair, G.E., Millner, P.A., 2010. *Anal. Chim. Acta* 681(1), 8–15.
- Dai, Z., Liu, S., Bao, J., Ju, H., 2009. *Chem. A Eur. J.* 15(17), 4321–4326.
- de Graaf, M., van Beek, J., Vennema, H., Podkolzin, A., Hewitt, J., Bucardo, F., Templeton, K., Mans, J., Nordgren, J., Reuter, G., 2015. *Eurosurveill.* 20(26), 1–8.
- Gao, L., Zhuang, J., Nie, L., Zhang, J., Zhang, Y., Gu, N., Wang, T., Feng, J., Yang, D., Perrett, S., 2007. *Nat. Nanotechnol.* 2(9), 577.
- Gupta, S., Huda, S., Kilpatrick, P.K., Velev, O.D., 2007. *Anal. Chem.* 79(10), 3810–3820.
- Haiss, W., Thanh, N.T., Aveyard, J., Fernig, D.G., 2007. *Anal. Chem.* 79(11), 4215–4221.
- Hall, A.J., Vinjé, J., Lopman, B., Park, G.W., Yen, C., Gregoricus, N., Parashar, U., 2011. *Morb. Mortal. Wkl. Rep.: Recomm. Rep.* 60(3), 1–15.
- Hao, N., Zhang, Y., Zhong, H., Zhou, Z., Hua, R., Qian, J., Liu, Q., Li, H., Wang, K., 2017. *Anal. Chem.* 89(19), 10133–10136.
- He, D., Garg, S., Waite, T.D., 2012a. *Langmuir* 28(27), 10266–10275.
- He, W., Zhou, Y.-T., Wamer, W.G., Boudreau, M.D., Yin, J.-J., 2012b. *Biomater.* 33(30), 7547–7555.
- Hou, W., Liu, X., Lu, Q., Liu, M., Zhang, Y., Yao, S., 2018. *Colloids Surf. B: Biointerfaces* 162, 118–125.
- Hwang, H.J., Ryu, M.Y., Park, C.Y., Ahn, J., Park, H.G., Choi, C., Ha, S.-D., Park, T.J., Park, J.P., 2017. *Biosens. Bioelectron.* 87, 164–170.
- Jones, A.M., Garg, S., He, D., Pham, A.N., Waite, T.D., 2011. *Environ. Sci. Technol.* 45(4), 1428–1434.

- Kitamoto, N., Tanaka, T., Natori, K., Takeda, N., Nakata, S., Jiang, X., Estes, M.K., 2002. *J. Clin. Microb.* 40(7), 2459–2465.
- Kou, B., Huang, W., Neill, F.H., Palzkill, T.G., Estes, M.K., Atmar, R.L., 2015. *J. Clin. Microb.*, JCM. 02371–02315.
- Lee, J., Adegoke, O., Park, E.Y., 2018. *Biotechnol. J.*, 1800249.
- Liu, R., Liu, X., Tang, Y., Wu, L., Hou, X., Lv, Y., 2011. *Anal. Chem.* 83(6), 2330–2336.
- Mays, G.P., Smith, S.A., 2011. *Health affairs (Project Hope)* 30(8), 1585–1593.
- Neethirajan, S., Ahmed, S.R., Chand, R., Buoziš, J., Nagy, E., 2017. *Nanotheranostics* 1(3), 272–295.
- Ni, P., Sun, Y., Dai, H., Hu, J., Jiang, S., Wang, Y., Li, Z., 2015. *Biosens. Bioelectron.* 63, 47-52.
- Parnklang, T., Lamlua, B., Gatemala, H., Thammacharoen, C., Kuimalee, S., Lohwongwatana, B., Ekgasit, S., 2015. *Mater. Chem. Phys.* 153, 127–134.
- Patel, M.M., Hall, A.J., Vinjé, J., Parashar, U.D., 2009. *J. Clin. Virol.* 44(1), 1–8.
- Samuni, A., Maimon, E., Goldstein, S., 2017. *Free Radic. Bio. Med.* 108, 832–839.
- Vashist, S.K., Luppa, P.B., Yeo, L.Y., Ozcan, A., Luong, J.H.T., 2015. *Trends Biotechnol.* 33(11), 692–705.
- Wang, S., Chen, W., Liu, A.L., Hong, L., Deng, H.H., Lin, X.H., 2012. *ChemPhysChem* 13(5), 1199–1204.
- Wang, S., Chen, Z., Choo, J., Chen, L., 2016. *Anal. Bioanal. Chem.* 408(4), 1015–1022.
- Xu, S., Ji, X., Xu, W., Li, X., Wang, L., Bai, Y., Zhao, B., Ozaki, Y., 2004. *Anal.* 129(1), 63–68.
- Yakes, B.J., Papafragkou, E., Conrad, S.M., Neill, J.D., Ridpath, J.F., Burkhardt III, W., Kulka, M., DeGrasse, S.L., 2013. *Int. J. Food Microb.* 162(2), 152–158.

Zheng, A.-X., Cong, Z.-X., Wang, J.-R., Li, J., Yang, H.-H., Chen, G.-N., 2013. *Biosens.*

Bioelectron. 49, 519–524.

Zhou, Z., Hao, N., Zhang, Y., Hua, R., Qian, J., Liu, Q., Li, H., Zhu, W., Wang, K., 2017.

Chem. Commun. 53(52), 7096-7099.

Figure Caption

Scheme 1. Proposed silver-enhanced nanozyme-based immunoassay

Fig. 1. Characteristic and physiochemical properties of Au/Ag NPs. (A) TEM image of Au NPs, (B) HR-TEM image of Au/Ag NPs. Red and yellow arrows indicate the Au core and Ag shell, respectively. (C) UV-Vis spectra of Au NPs (black) and Au/Ag NPs (red). (D) Zeta potential (red) and hydrodynamic size (blue) of Au/Ag NPs based on the concentration of AgNO₃. (E) XRD analysis.

Fig. 2. Comparison of the peroxidase-like activity of the nanomaterials (A) and protein-coated nanomaterials (B). The maximal reaction rate was calculated based on the concentration of TMB_{ox} ($l=0.76$ cm) at $t=1$ min based on the absorbance of the reaction. The red circles and black squares in (A) indicate Au/Ag NPs and Au NPs, respectively. The blue and open circles and closed squares in (B) indicate protein-coated Au/Ag core/shell NPs, Au/protein-coated Ag core/shell NPs and protein-coated Au NPs, respectively.

Fig. 3. Proposed silver-enhanced peroxidase-like activity of in-situ Au/Ag NPs. (A) Formation of in-situ Au/Ag core/shell NPs and (B) Release of Ag⁺ of Au/Ag NPs in H₂O₂/TMB and catalytic oxidation of TMB.

Fig. 4. Detection of NoV-LPs. (A) Selectivity test (inset: color developed in the well). (B) Calibration curve based on the concentration of NoV-LPs using different NoV-LP concentrations. The error bars indicate the standard deviation (SD) of the experiment ($n=3$). The red circles, black squares and open circles denote the enhanced colorimetric immunoassay, HRP-based ELISA and Au NPs-based colorimetric immunoassay, respectively.

Fig. 5. Detection of (A) NoV GII.4 and (B) NoV GII.3. The red circles and open squares denote the enhanced colorimetric immunoassay and commercial NoV detection kit, respectively. The upper and lower inset images in A and B show the developed color in the enhanced colorimetric immunoassay and commercial NoV detection kit, respectively. (+) in the inset images in A and B indicate the positive control for the commercial NoV detection kit. The error bars indicate the standard deviation (SD) of the experiment (n=3).

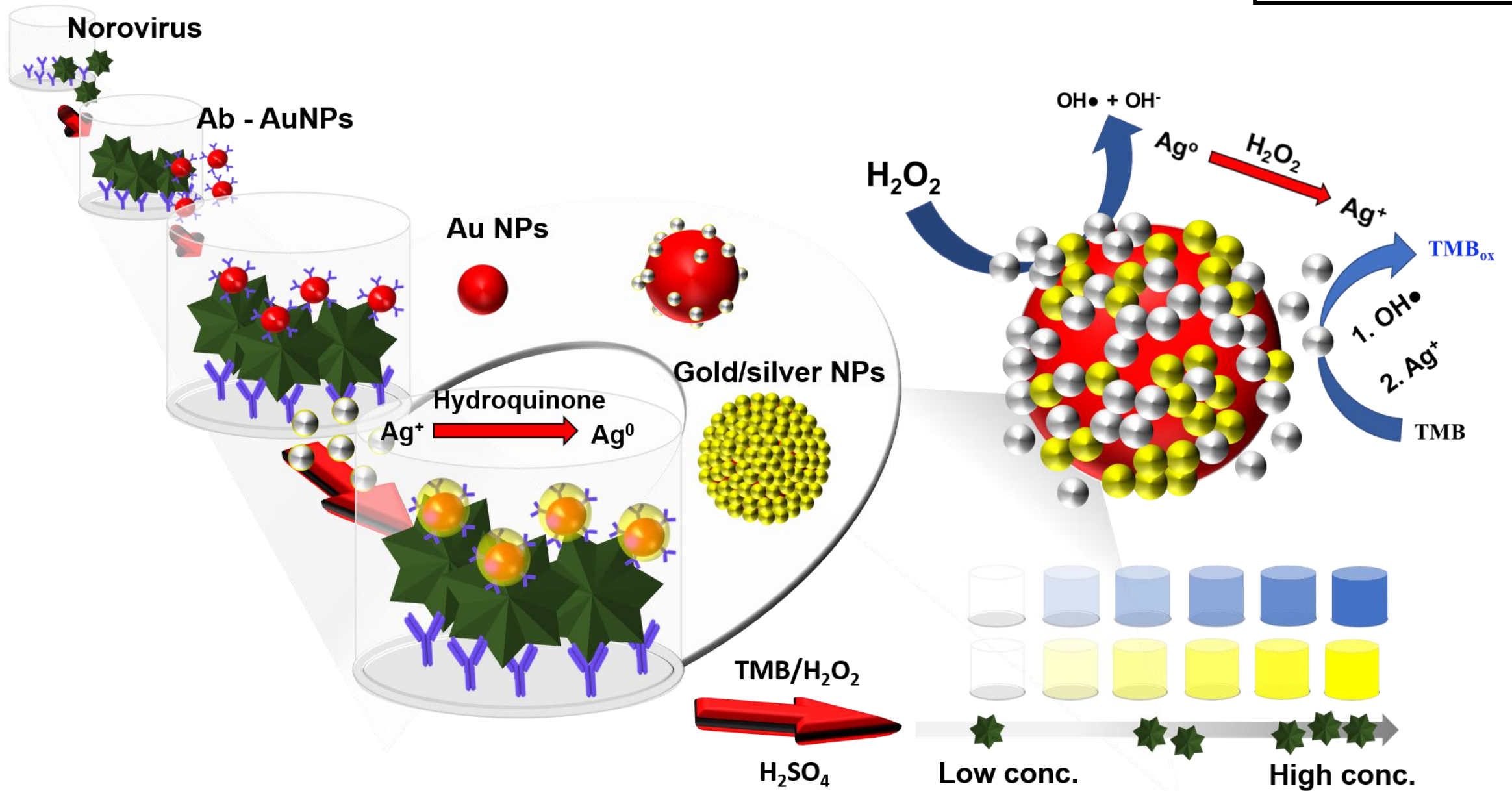
Table 1

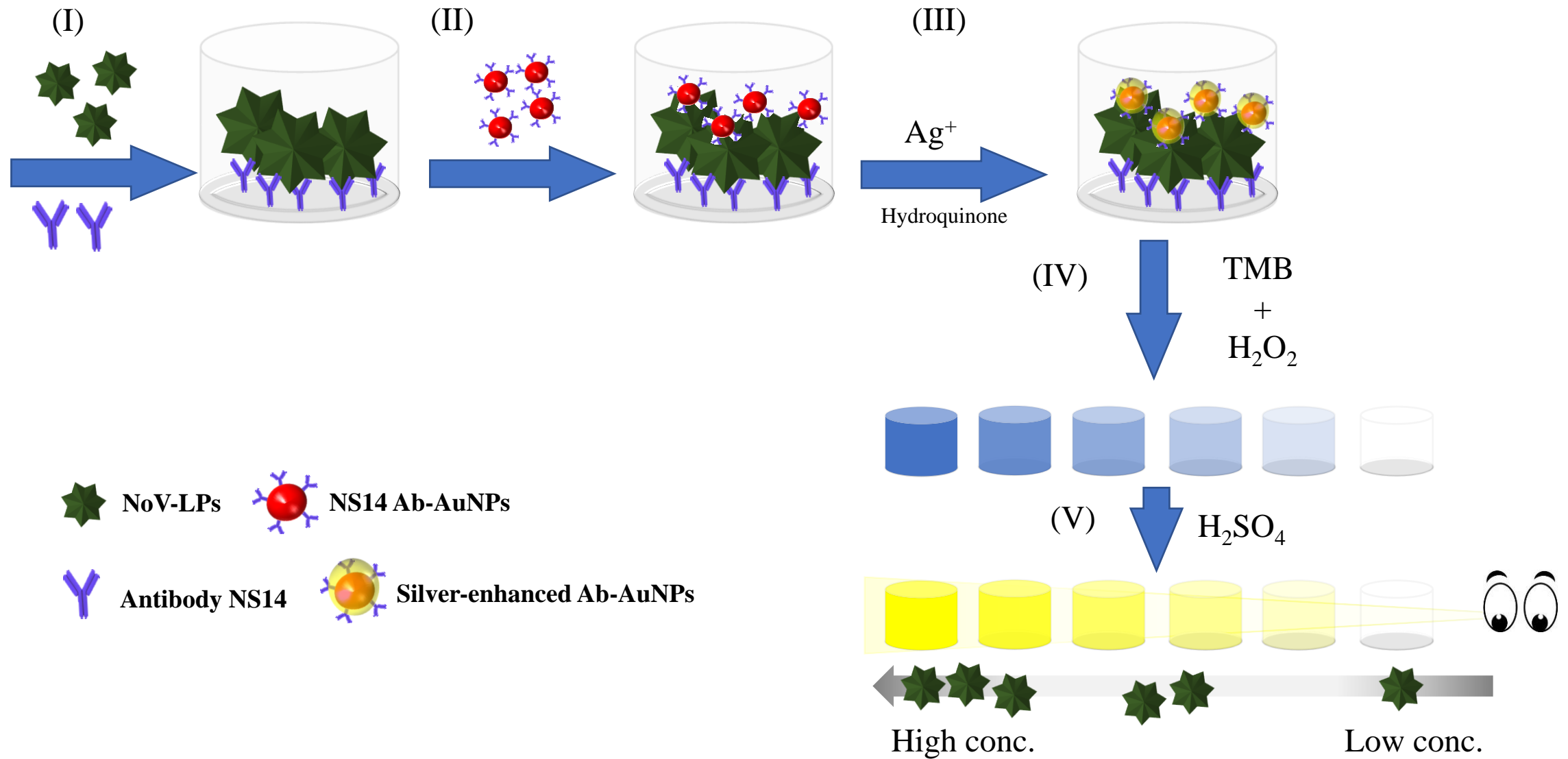
Kinetic parameters of Au NPs and Au/Ag NPs.

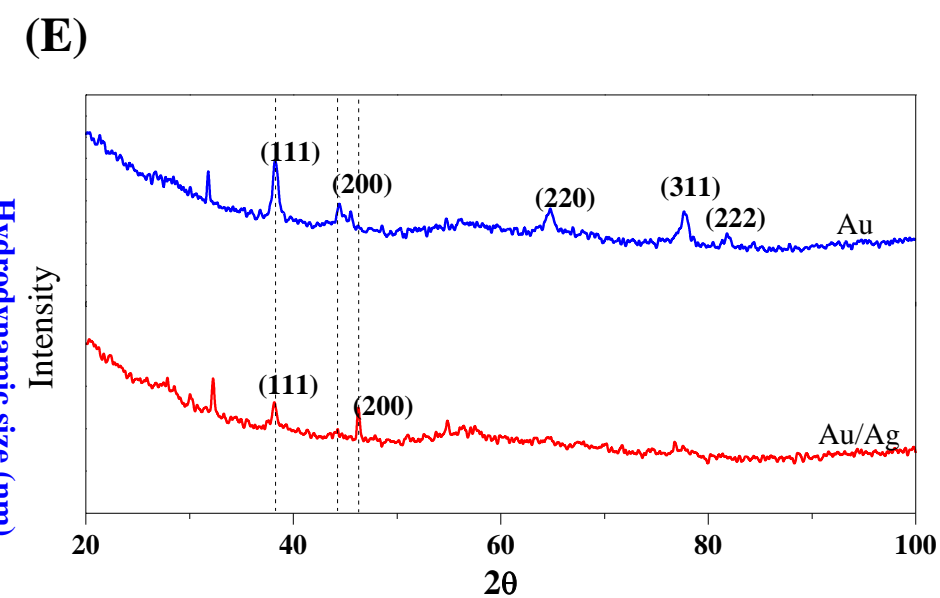
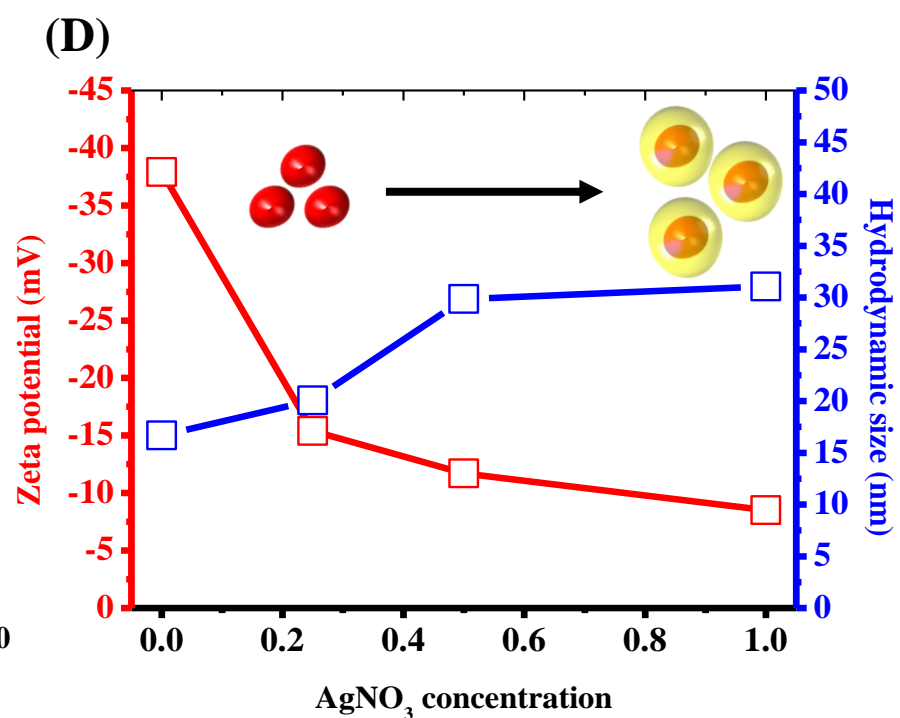
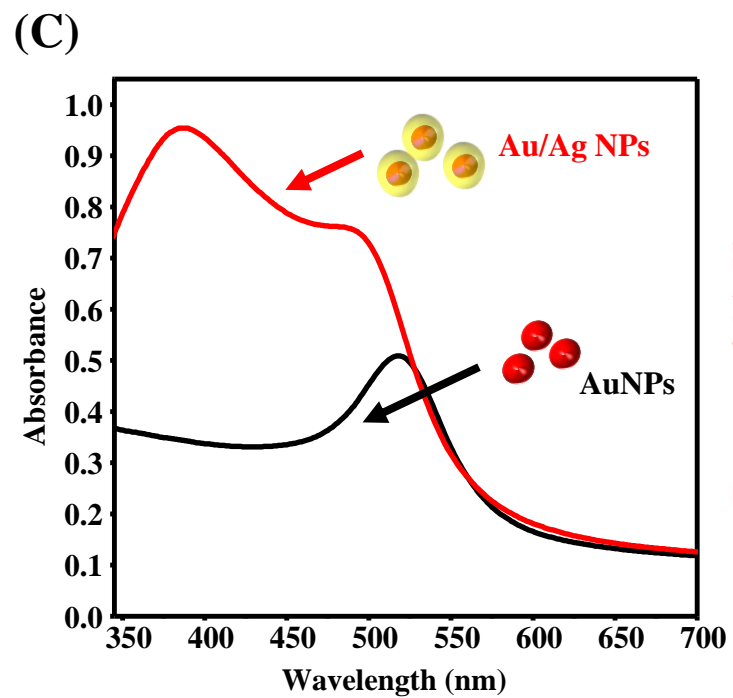
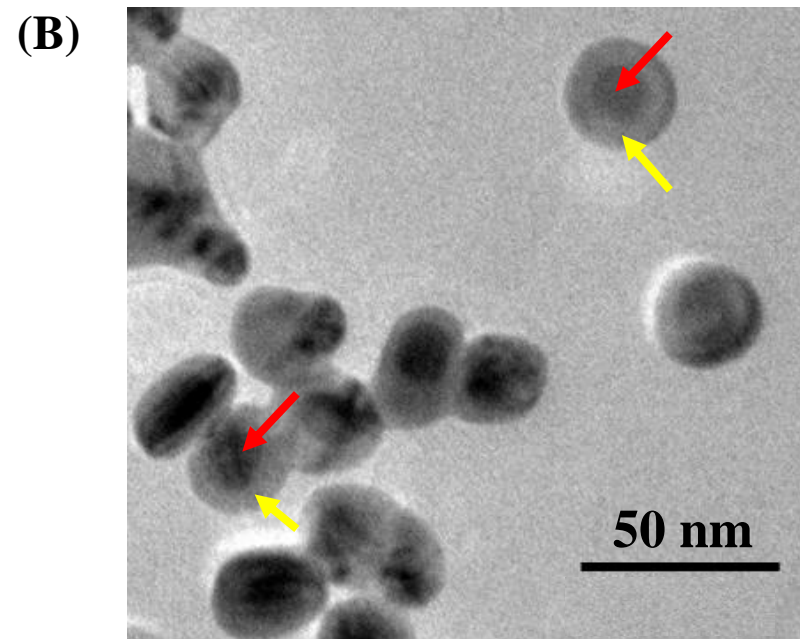
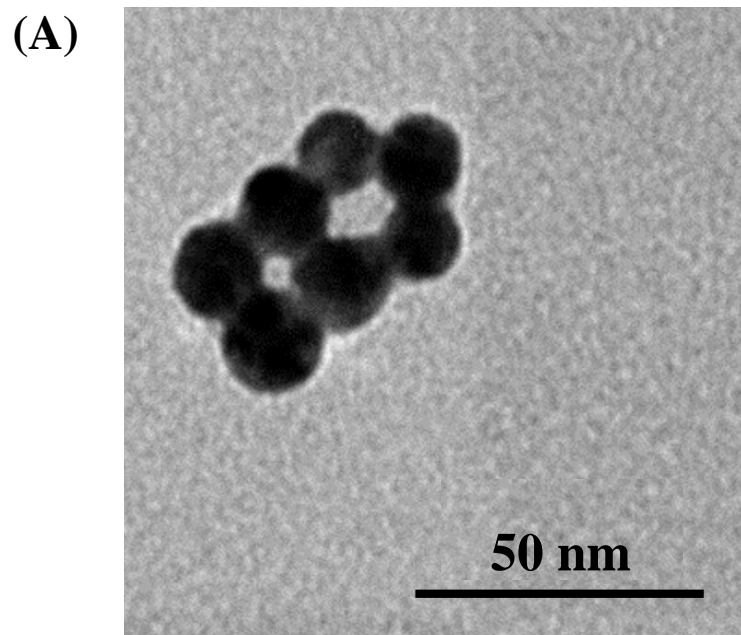
TMB	K_m (mM)	V_m ($\times 10^9$ mM s⁻¹)	k_{cat} (s⁻¹)	k_{cat}/K_m (mM⁻¹ s⁻¹)
Au NPs	10.020	282.0	367.82	36.71
Au/Ag NPs	0.155	4.1	5.38	34.67

H₂O₂	K_m (mM)	V_m ($\times 10^9$ mM s⁻¹)	k_{cat} (s⁻¹)	k_{cat}/K_m (mM⁻¹ s⁻¹)
Au NPs	3.456	72.0	94.70	27.40
Au/Ag NPs	0.092	2.9	3.81	41.35

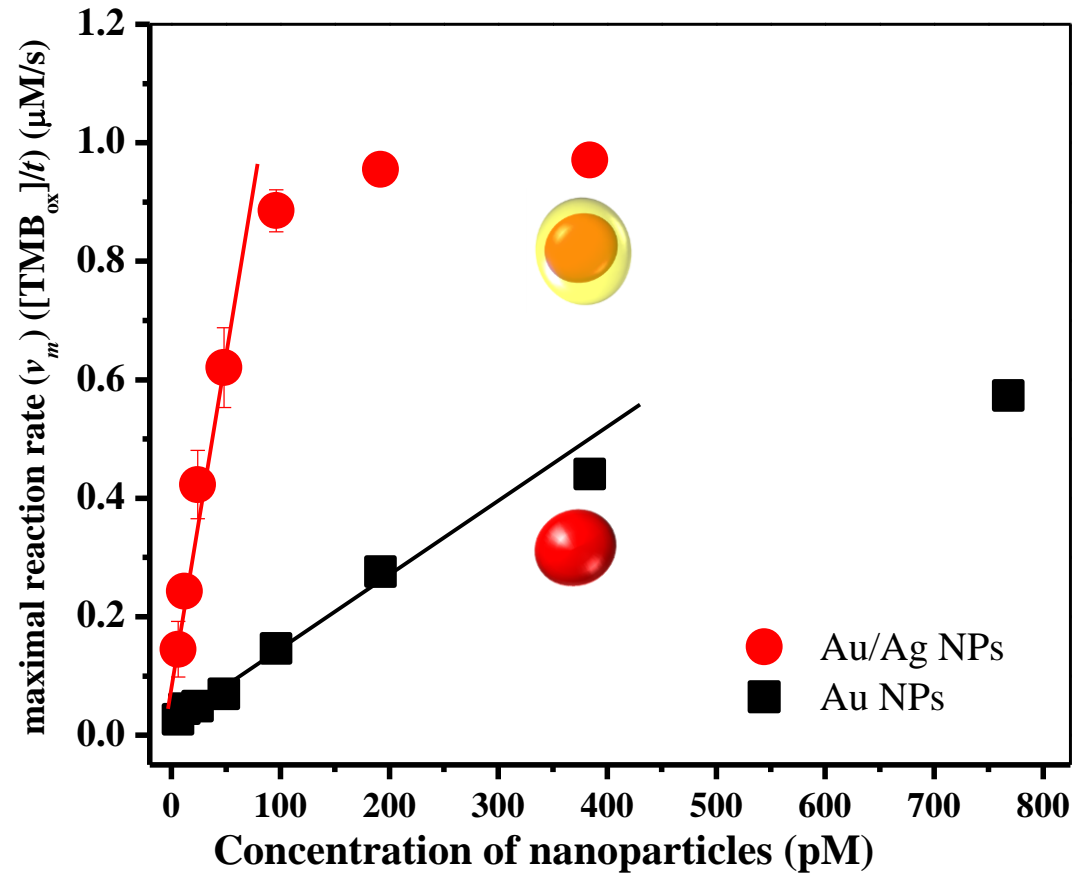
The concentration of nanomaterials used was 7.68×10^{-10} M.



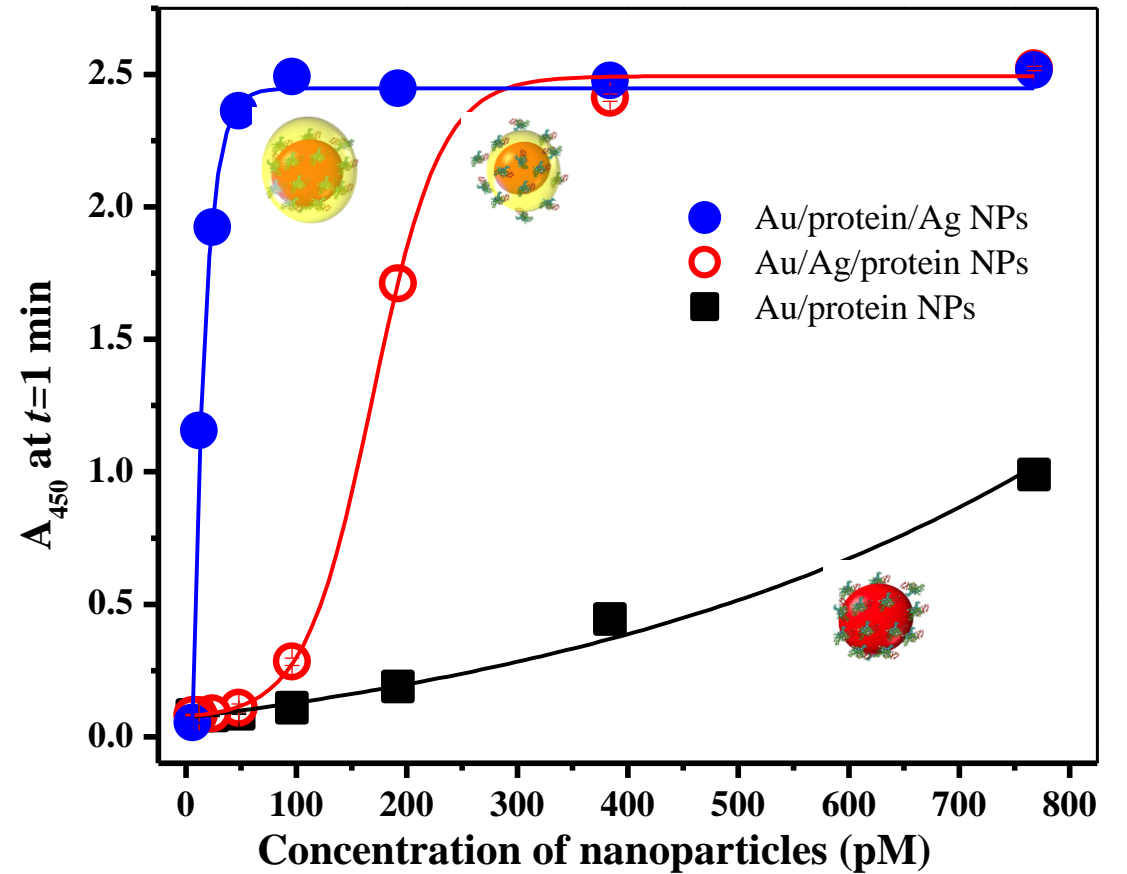


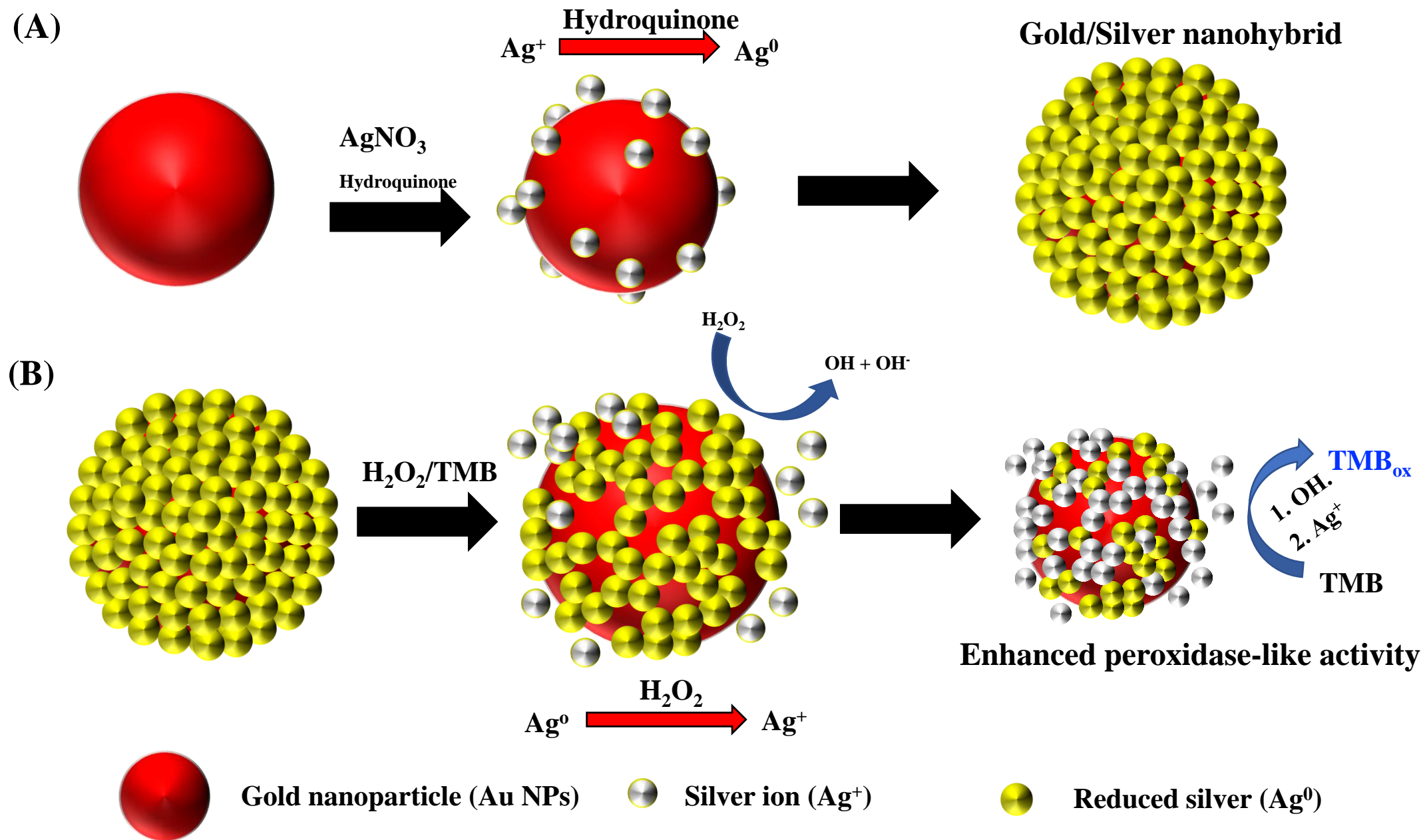


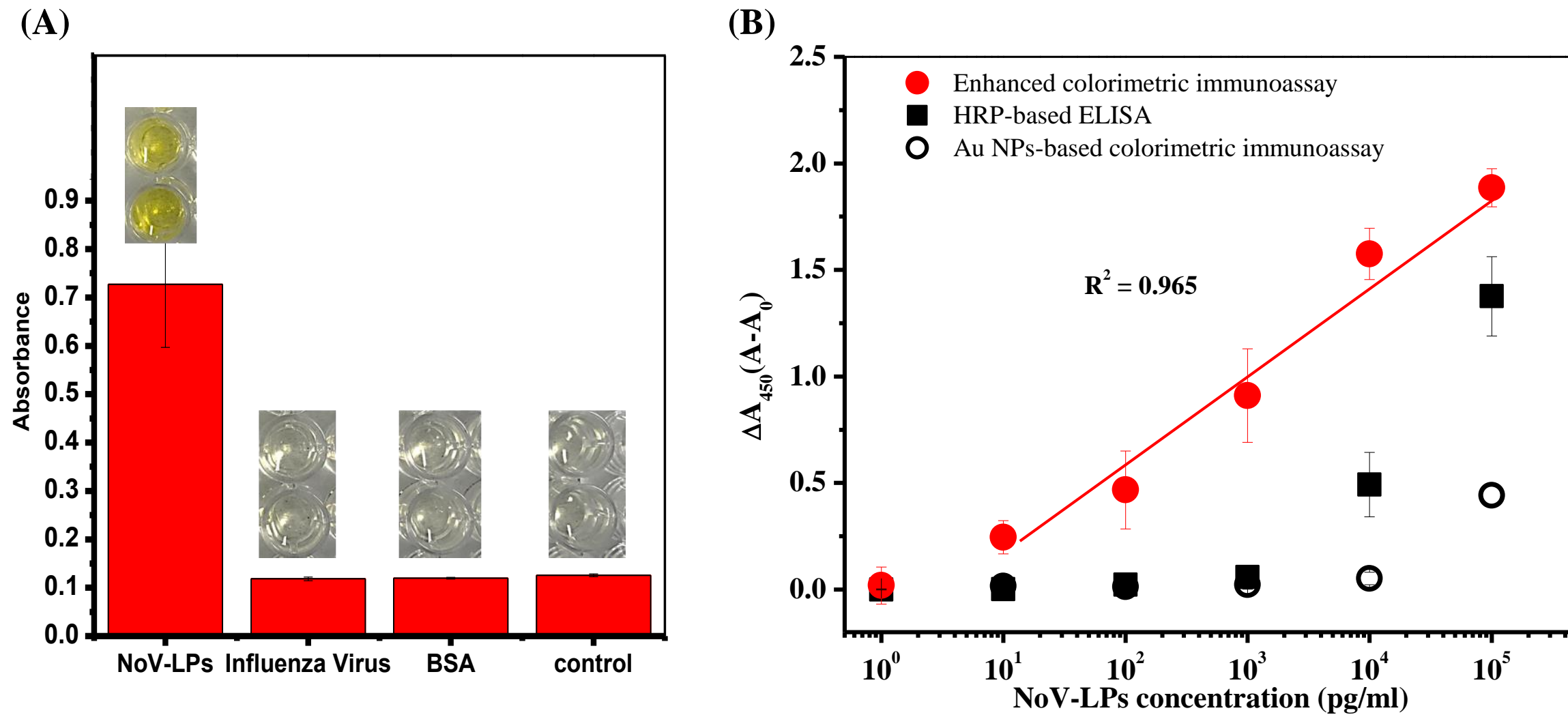
(A)



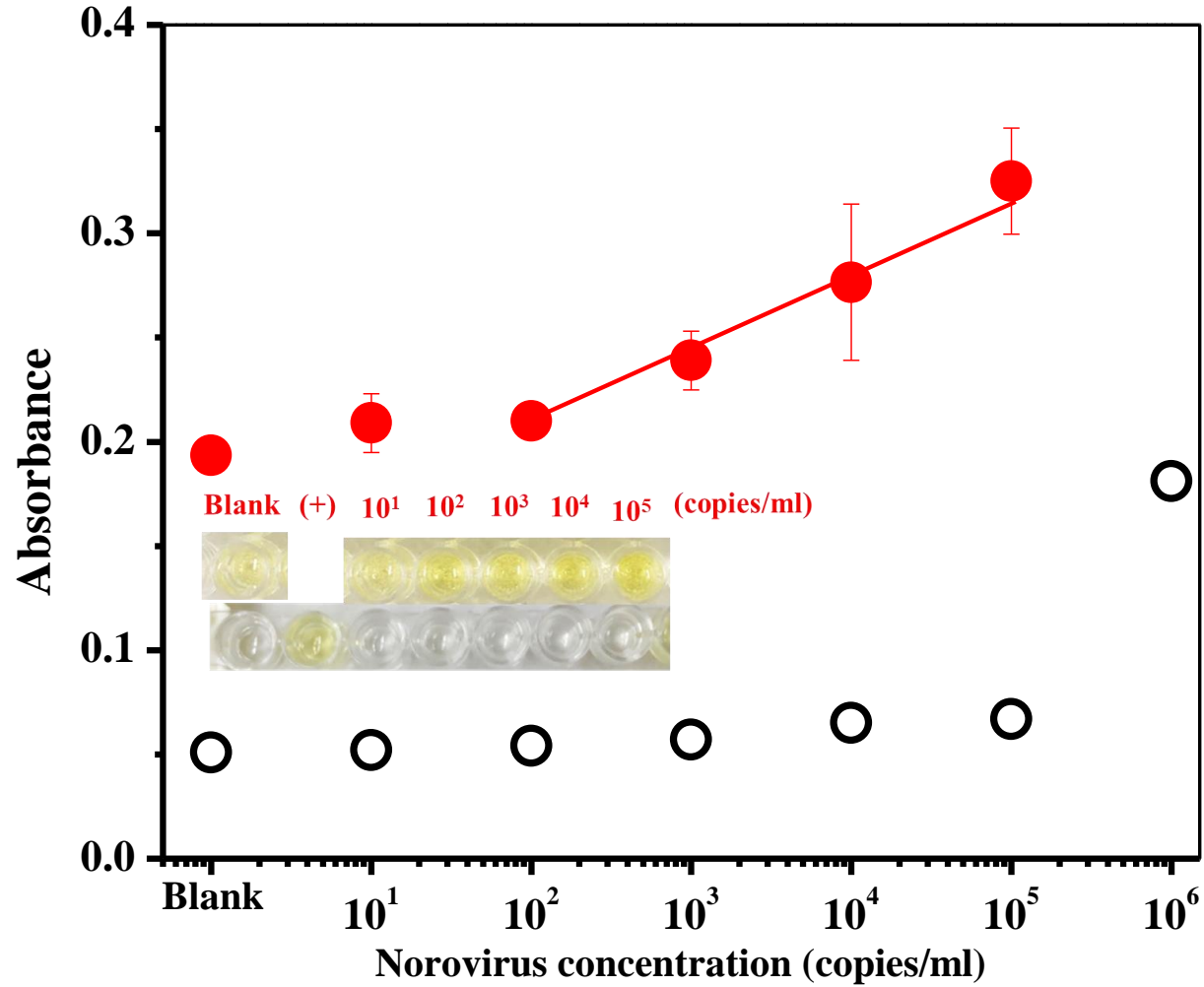
(B)



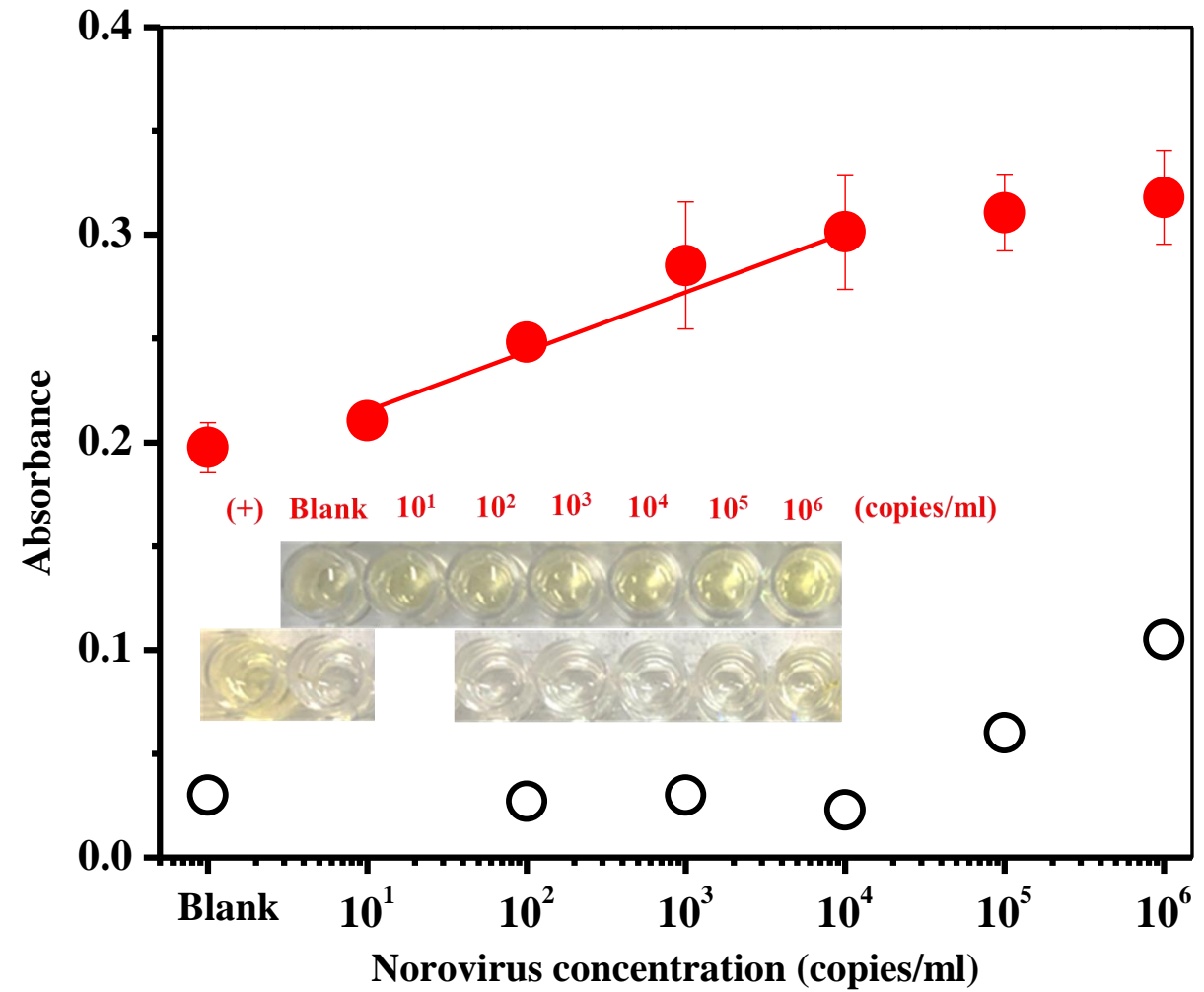




(A)



(B)



Supplement Information

Enhanced colorimetric detection of norovirus using in-situ growth of Ag shell on Au NPs

Indra Memdi Khoris^a, Kenshin Takemura^b, Jaewook Lee^{c,†}, Toshimi Hara^d, Fuyuki Abe^d, Tetsuro Suzuki^e, Enoch Y. Park^{*,a,b,c}

^a *Department of Applied Biological Chemistry, College of Agriculture, Graduate School of Integrated Science and Technology, Shizuoka University, 836 Ohya, Suruga-ku, Shizuoka 422-8529, Japan*

^b *Department of Bioscience, Graduate School of Science and Technology, Shizuoka University, 836 Ohya, Suruga-ku, Shizuoka 422-8529, Japan*

^c *Research Institute of Green Science and Technology, Shizuoka University, 836 Ohya, Suruga-ku, Shizuoka 422-8529, Japan*

^d *Department of Microbiology, Shizuoka Institute of Environment and Hygiene, 4-27-2, Kitando, Aoi-ku, Shizuoka 420-8637, Japan*

^e *Department of Infectious Disease, Hamamatsu University School of Medicine, 1-20-1 Higashi-ku, Handa-yama, Hamamatsu 431-3192, Japan*

E-mail:

indra.memdi.khoris.17@shizuoka.ac.jp (IMK)

takemura.kenshin.16@shizuoka.ac.jp (KT)

nanojaewook@outlook.com (JL)

toshimi1_hara@pref.shizuoka.lg.jp (TH)

fuyuki1_abe@pref.shizuoka.lg.jp (FA)

tesuzuki@hama-med.ac.jp (TS)

park.enoch@shizuoka.ac.jp (EYP)

* Corresponding author: Research Institute of Green Science and Technology, Shizuoka University, 836 Ohya, Suruga-ku, Shizuoka 422-8529, Japan.

E-mail address: park.enoch@shizuoka.ac.jp (E.Y. Park). Tel (Fax): +81-54-238-4887

† Current address; School of Materials Science, Japan advanced Institute of science and Technology, Asahidai 1-1, Nomishi, Ishikawa 923-1292, Japan

Table S1. Silver reaction in H₂O₂/TMB solution

Reactions	Equation	Ref.
$Ag + H_2O_2 \rightarrow Ag^+ + OH \cdot + OH^-$	(1)	(Hou et al. 2018)
$H_2O_2 + OH^- \rightarrow HO_2^- + H_2O$	(2)	(He et al. 2012)
$2Ag^+ + HO_2^- + OH^- \rightarrow 2Ag + O_2 + H_2O$	(3)	(He et al. 2012)
$TMB + OH \cdot \rightarrow TMB_{ox} + H_2O$	(4)	(Bhagat et al. 2018)
$TMB + H_2O_2 \rightarrow TMB_{ox} + H_2O$ (presence of Au NPs)	(5)	(Ahmed et al. 2017)
$TMB + Ag^+ \rightarrow TMB_{ox} + Ag$	(6)	(Ni et al. 2015)

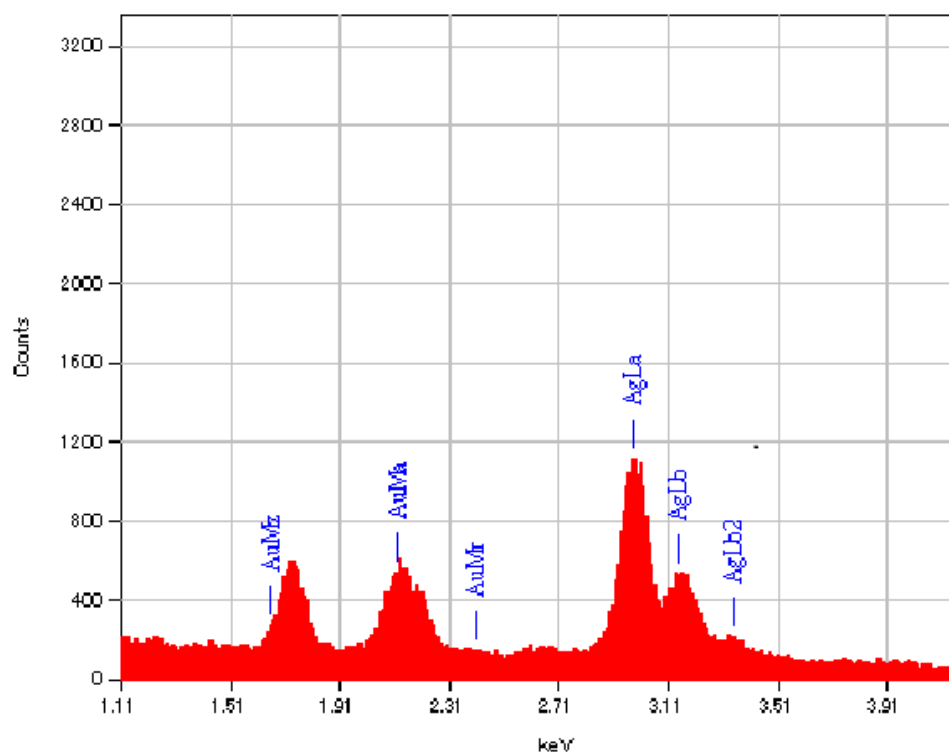


Figure S1. EDS analysis of Au/Ag NPs

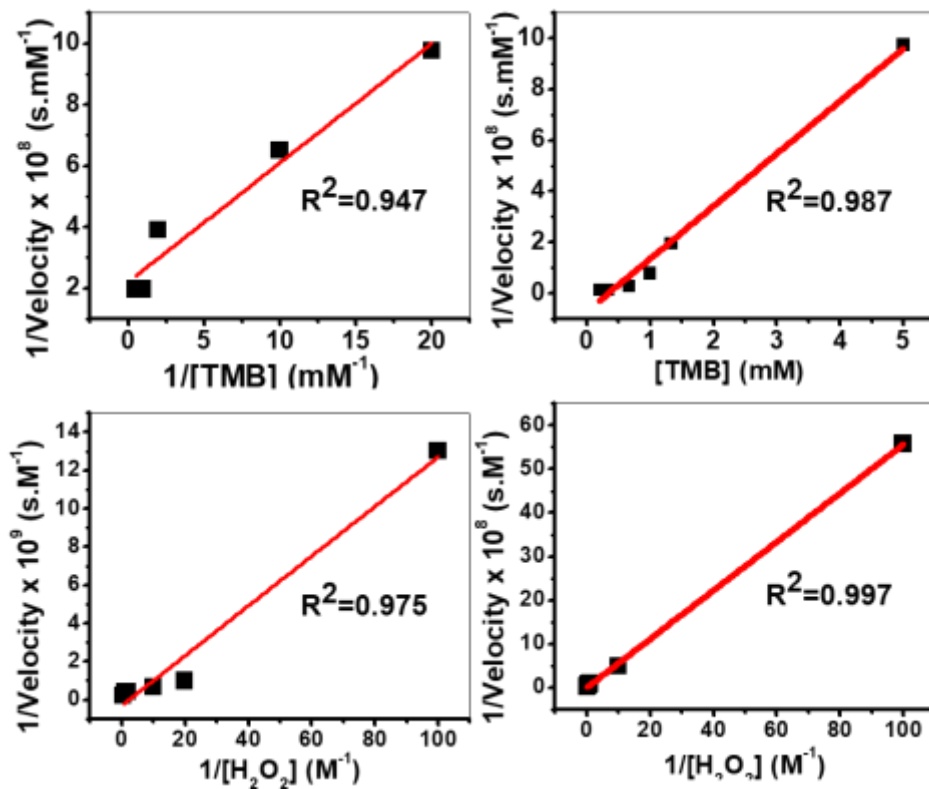


Figure S2. Lineweaver-Burk plot of peroxidase-like activity of nanomaterials. (Left side: Au/Ag NPs and right side: Au NPs)

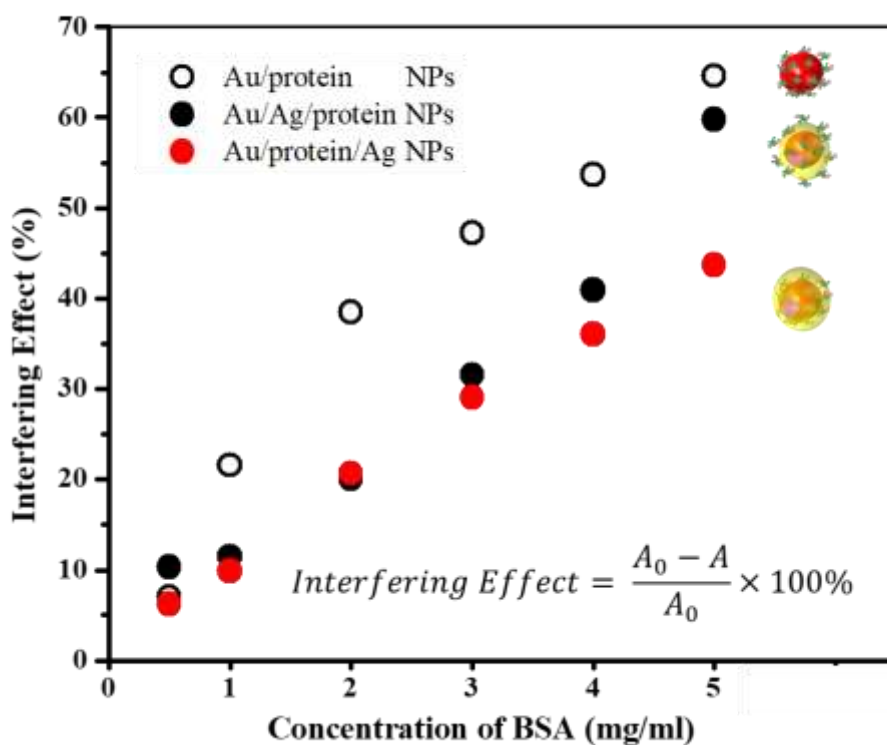


Figure S3. Protein blocking effect on catalytic activity of nanomaterials. Nanomaterials were incubated in defined concentration of bovine serum albumin (BSA) and separated uncoated proteins by centrifugation prior to catalytic reaction in TMB/H₂O₂ solution. A and A_0 denote values with and without protein blocking, respectively. Open, black and red circles denote Au NPs, Au/Ag core/shell NPs and in-site Au/Ag core/shell NPs, respectively.

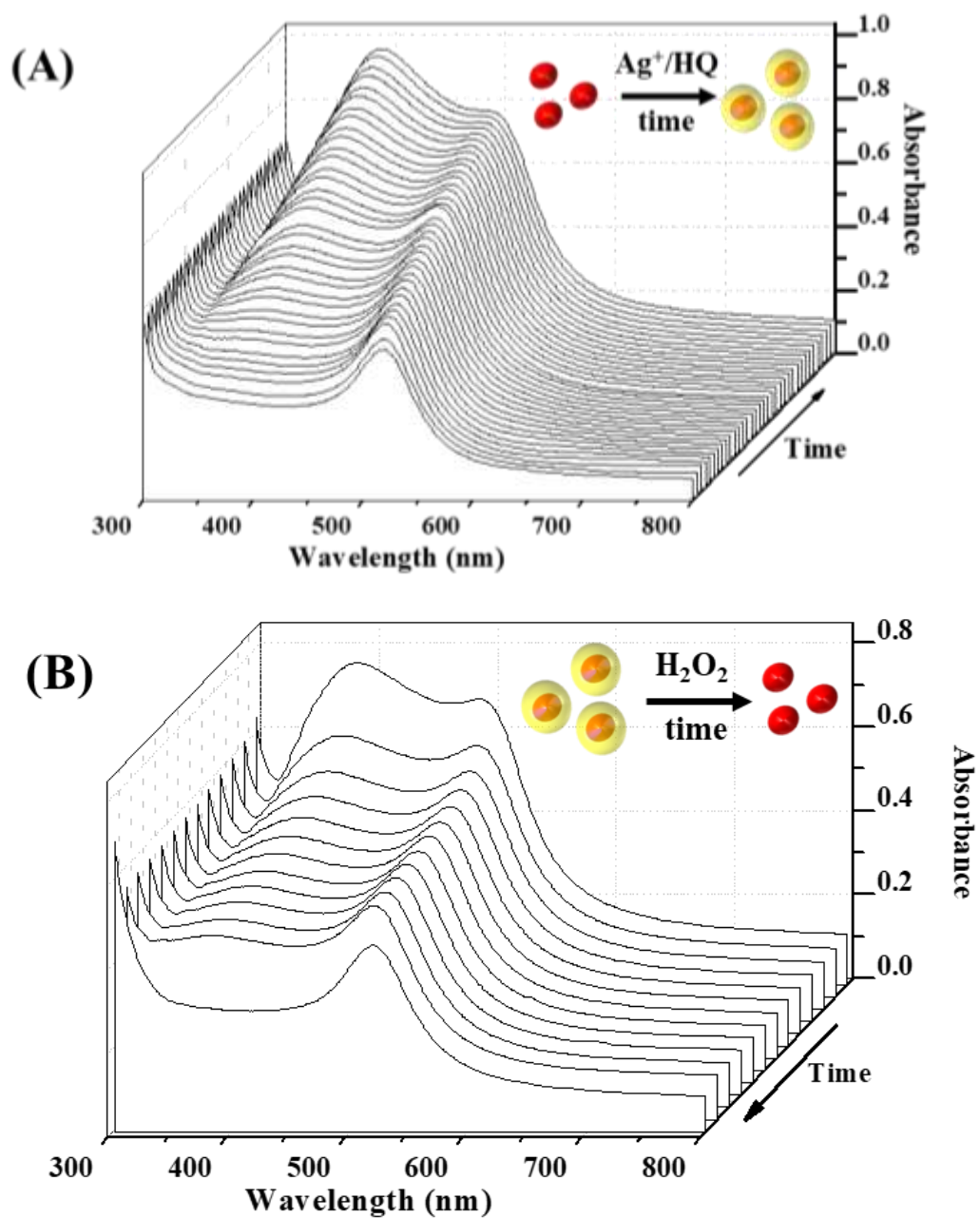


Figure S4. (A) Absorbance spectrum of formation of Au/Ag NPs over time, (B) Absorbance spectrum of deformation of Au/Ag NPs by H₂O₂ over time.

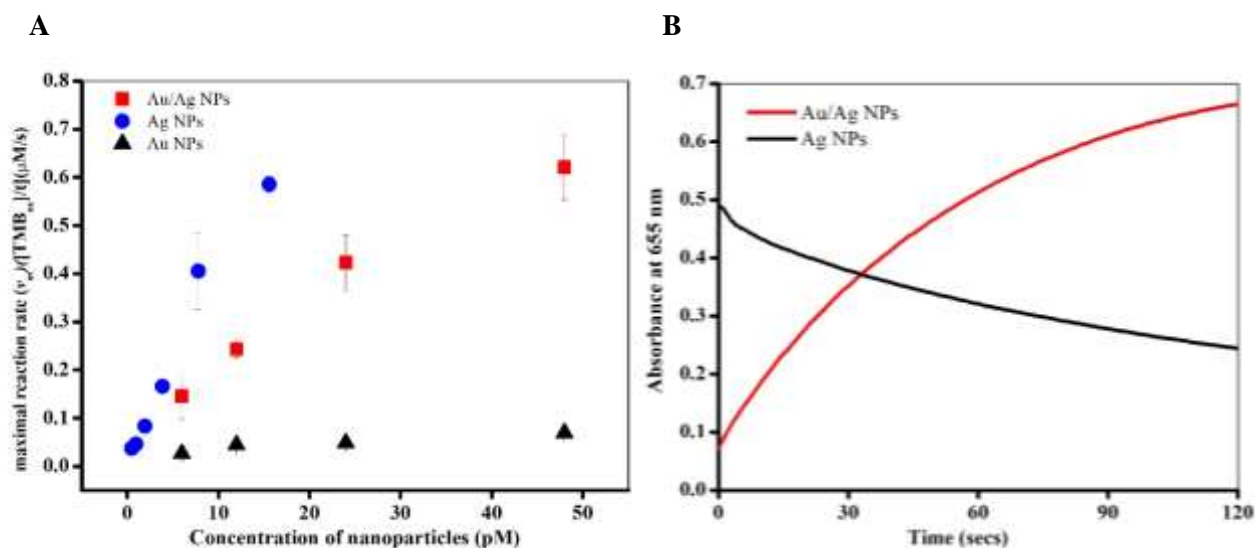


Figure S5. Ag NPs reaction to $\text{H}_2\text{O}_2/\text{TMB}$ system. (A) Based on NPs concentration and (B) time-dependent reaction of Ag NPs and Au/Ag NPs. Y-axis in (A) represents maximal reaction rate which was calculated from A_{450} of TMB_{ox} using beer-lambert law and Y-axis in (B) represents A_{655} of charge complex of TMB and TMB_{ox} .

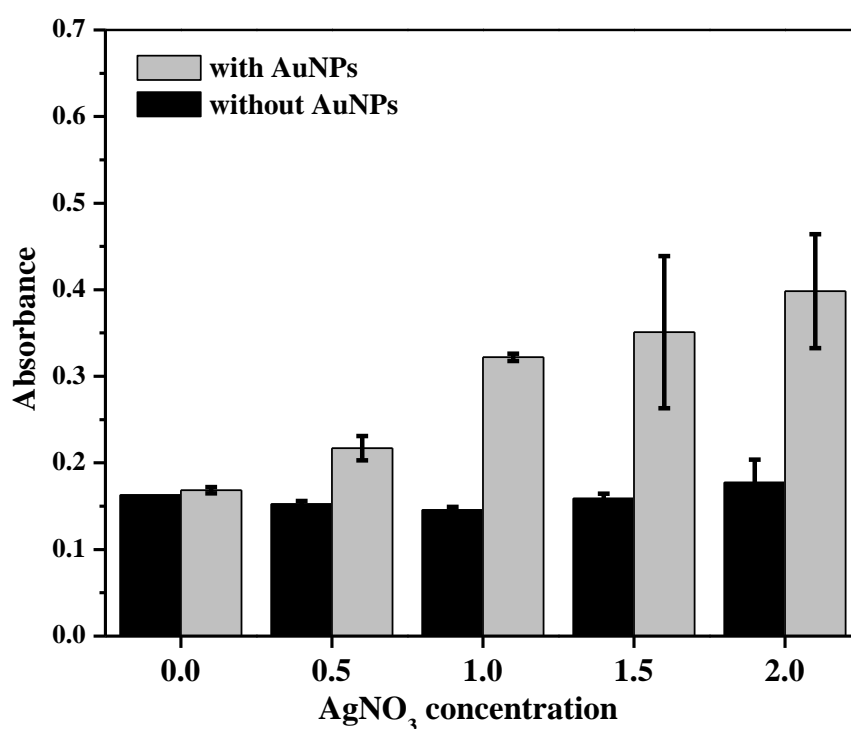


Figure S6. Optimization of silver nitrate (AgNO_3) concentration using skimmed milk as coated protein in the absence (black bars) and present (grey bars) of AuNPs

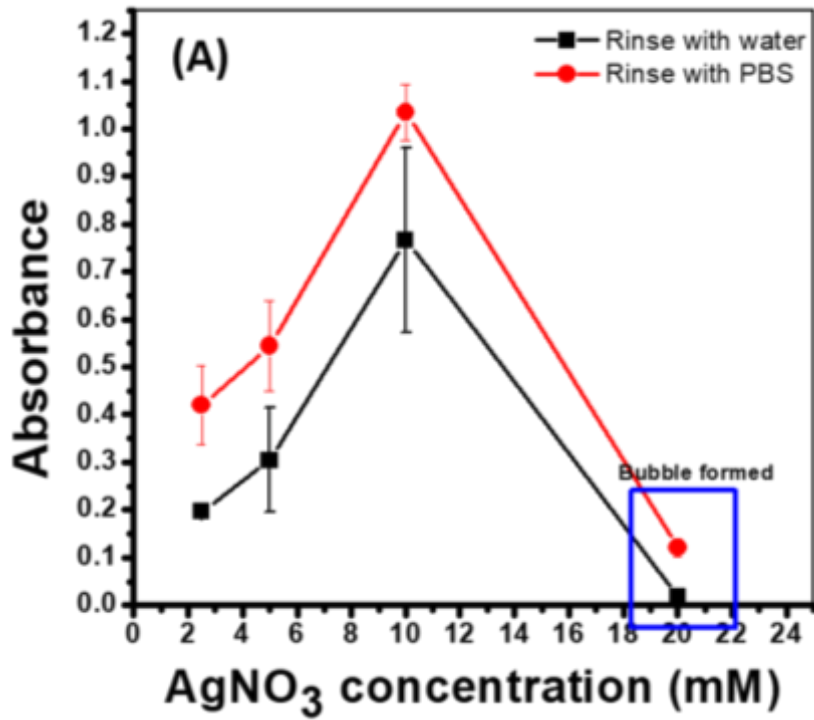


Figure S7. Different washing buffer in the assay.

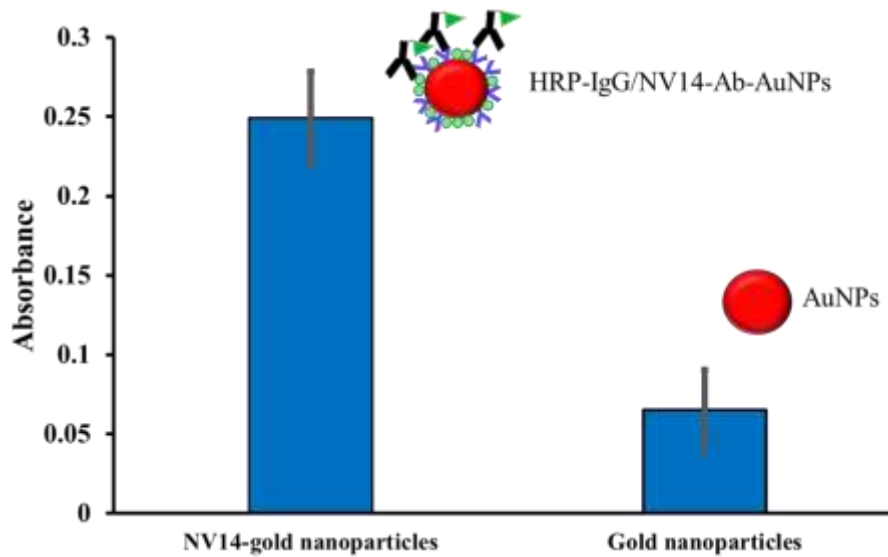


Figure S8. Confirmation of Antibody NV14 (Ab-NV14) conjugated nanoparticles (AuNPs). The absorbance was measured at 450 nm

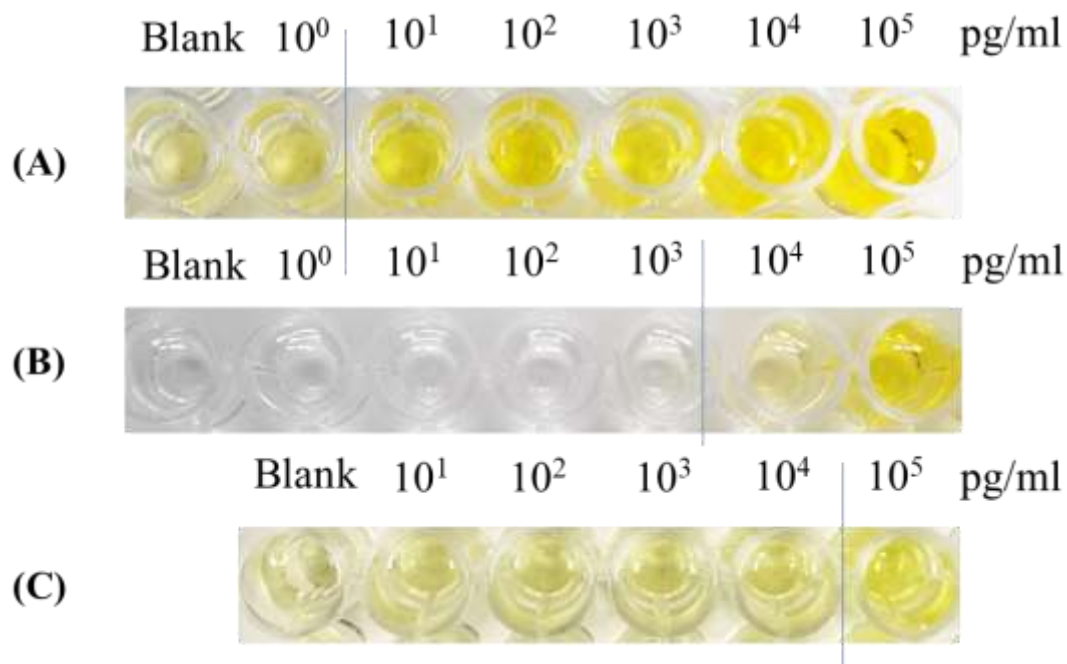


Figure S9. Detection result of norovirus-like particles using (A) Au/Ag nanohybrid NPs, (B) NV14 Ab-HRP-IgG system and (C) Au NPs. ($t=1$ min). (Absorbance measurement was plotted in Figure 4B). Blue line was drawn to show the observable colour

Reference

- Ahmed, S.R., Takemeura, K., Li, T.-C., Kitamoto, N., Tanaka, T., Suzuki, T., Park, E.Y., 2017. *Biosens. Bioelectron.* 87, 558–565.
- Bhagat, S., Vallabani, N.S., Shutthanandan, V., Bowden, M., Karakoti, A.S., Singh, S., 2018. *J. Colloid Interface Sci.* 513, 831–842.
- He, W., Zhou, Y.-T., Wamer, W.G., Boudreau, M.D., Yin, J.-J., 2012. *Biomater.* 33(30), 7547–7555.
- Hou, W., Liu, X., Lu, Q., Liu, M., Zhang, Y., Yao, S., 2018. *Colloids Surf. B: Biointerfaces* 162, 118–125.
- Ni, P., Sun, Y., Dai, H., Hu, J., Jiang, S., Wang, Y., Li, Z., 2015. *Biosens. Bioelectron.* 63, 47–52.